UC San Diego

UC San Diego Previously Published Works

Research

Effects of Early Life Oral Arsenic Exposure on Intestinal Tract Development and Lipid Homeostasis in Neonatal Mice: Implications for NAFLD Development

Xiaojing Yang,[1] André A. Weber,[1] Elvira Mennillo,[1] Patrick Secrest,[2] Max Chang,[3] Samantha Wong,[1] Sabrina Le,[1] Junlai Liu,[4] Christopher W. Benner,[3] Michael Karin,[4] Philip L.S.M. Gordts,[2] Robert H. Tukey,[1] and Shujuan Chen[1]

[1]Laboratory of Environmental Toxicology, Department of Pharmacology, University of California, San Diego (UC San Diego), La Jolla, California, USA
[2]Department of Medicine, Division of Endocrinology and Metabolism, UC San Diego, La Jolla, California, USA
[3]Department of Medicine, School of Medicine, UC San Diego, La Jolla, California, USA
[4]Laboratory of Gene Regulation and Signal Transduction, Department of Pharmacology, UC San Diego, La Jolla, California, USA

BACKGROUND: Newborns can be exposed to inorganic arsenic (iAs) through contaminated drinking water, formula, and other infant foods. Epidemiological studies have demonstrated a positive association between urinary iAs levels and the risk of developing nonalcoholic fatty liver disease (NAFLD) among U.S. adolescents and adults.

OBJECTIVES: The present study examined how oral iAs administration to neonatal mice impacts the intestinal tract, which acts as an early mediator for NAFLD.

METHODS: Neonatal mice were treated with a single dose of iAs via oral gavage. Effects on the small intestine were determined by histological examination, RNA sequencing, and biochemical analysis. Serum lipid profiling was analyzed by fast protein liquid chromatography (FPLC), and hepatosteatosis was characterized histologically and biochemically. Liver X receptor-alpha (LXRα) knockout ($Lxr\alpha^{-/-}$) mice and liver-specific activating transcription factor 4 (ATF4)-deficient ($Atf4^{\Delta Hep}$) mice were used to define their roles in iAs-induced effects during the neonatal stage.

RESULTS: Neonatal mice exposed to iAs via oral gavage exhibited accumulation of dietary fat in enterocytes, with higher levels of enterocyte triglycerides and free fatty acids. These mice also showed accelerated enterocyte maturation and a longer small intestine. This was accompanied by higher levels of liver-derived very low-density lipoprotein and low-density lipoprotein triglycerides, and a lower level of high-density lipoprotein cholesterol in the serum. Mice exposed during the neonatal period to oral iAs also developed hepatosteatosis. Compared with the control group, iAs-induced fat accumulation in enterocytes became more significant in neonatal $Lxr\alpha^{-/-}$ mice, accompanied by accelerated intestinal growth, hypertriglyceridemia, and hepatosteatosis. In contrast, regardless of enterocyte fat accumulation, hepatosteatosis was largely reduced in iAs-treated neonatal $Atf4^{\Delta Hep}$ mice.

CONCLUSION: Exposure to iAs in neonatal mice resulted in excessive accumulation of fat in enterocytes, disrupting lipid homeostasis in the serum and liver, revealing the importance of the gut–liver axis and endoplasmic reticulum stress in mediating iAs-induced NAFLD at an early age. https://doi.org/10.1289/EHP12381

Introduction

Inorganic arsenic (iAs) is a naturally occurring metalloid that has adverse effects on human health, mainly owing to exposure mediated by drinking water.[1] When iAs contaminates well water, its concentration can reach hundreds of micrograms per liter,[2] far exceeding the U.S. Environmental Protection Agency's (EPA) water quality standard of $<10 \mu g/L$.[3] In addition, groundwater and soil can accumulate iAs through irrigation, further contaminating the food chain.[4] Foods, including apple juice, chicken, wine, and beer, have been shown to be contaminated with iAs.[5] Rice accumulates more iAs than other food sources, with high levels detected in rice-based products such as rice milk, rice-based breakfast cereals, and infant rice cereal.[6–9] Humans at all ages can be exposed to iAs, starting *in utero* given that it can readily pass the placenta into the fetus.[10,11] The effects of fetal exposure to iAs may be exacerbated by postnatal exposure through formula or infant food prepared with water contaminated by iAs. Relative to body weight (BW), infants in the first 6 months of life drink seven times as much water, and 1- to 5-y-old children eat three to four times more food than the average adult.[12–14] This disproportionate exposure may result in higher-than-expected levels of iAs in children as demonstrated by elevated blood iAs levels not predictable by home water iAs levels.[15]

The incidence of fatty liver disease (FLD), whether driven by alcohol (AFLD) or not[16] [i.e., nonalcoholic FLD (NAFLD) driven by type 2 diabetes and obesity[17] or toxicant-associated FLD (TAFLD)[18]] has greatly increased in the past 50 y, such that $\sim 30\%$ of U.S. adults are affected by some form of FLD, most often NAFLD.[19] NAFLD is the leading chronic liver disease worldwide, affecting people of all ages, from young children to adolescents to adults.[20,21] The early signs of NAFLD include hepatosteatosis (fat accumulates in liver), a benign condition that exhibits few or no symptoms. As steatosis progresses, inflammatory cells infiltrate and damage liver cells, causing nonalcoholic steatohepatitis, with the potential for progression to fibrosis, cirrhosis, and hepatocellular carcinoma.[22] NAFLD is commonly associated with metabolic risk factors, and the global prevalence of NAFLD has been paralleled by increasing rates of obesity and type 2 diabetes.[23] Along with hypernutrition being a prerequisite for steatosis, environmental and industrial chemicals are reported to be associated with fatty liver injury, with TAFLD displaying pathological similarities to NAFLD.[18,24] The association between TAFLD and exposure to hepatotoxic chemicals in the absence of underlying overnutrition has been established.[25] Epidemiological studies from the National Health and Nutrition Examination Survey (2005–2014)[26] confirmed an association between urinary iAs levels and the risk of NAFLD among U.S. adolescents and adults.

NAFLD in adults and children (pediatric NAFLD) share many common features in the pathogenesis and disease progression, but several important differences have been identified.[27] When evaluating biopsies from 100 children 2–18 years of age with biopsy-proven NAFLD, the Schwimmer laboratory at the University of California, San Diego (UCSD), reported[28] two prevalent phenotypes: *a*) type 1 (adult-type), present in 17% of children, which was characterized by steatosis distributed in the

pericentral region (zone 3); and *b*) type 2 (pediatric-type), which is present in 51% of children and characterized by steatosis in the periportal region (zone 1). A further cross-sectional study of 813 children (<18 years of age; mean = 12.8 ± 2.7 y) with NAFLD[29] confirmed that zone 1 steatosis, although rare in adults with NAFLD, was found in children. It was identified that the only independent risk factor for having zone 1 steatosis was age, with a significantly higher percentage found in younger children. Children with zone 1 steatosis also had a significantly higher proportion with any fibrosis compared with those with zone 3 steatosis.[29] These results further highlight the time sensitivity in NAFLD pathogenesis.

To determine the effects of iAs exposure on lipid metabolism and NAFLD during the early developmental stage, this study employed RNA sequencing, fast protein liquid chromatography (FPLC), and diverse histological analysis. We also used global Liver X receptor-alpha (LXRα) knockout ($Lxr\alpha^{-/-}$) mice and liver-specific ATF4-deficient ($Atf4^{\Delta Hep}$) mice to further understand the underlying mechanisms of iAs-induced NAFLD.

Methods

Animal Strains

All mice used in these experiments were of a C57BL/6J background with in-house breeding. Wild-type (WT) C57BL/6J mice were purchased from Charles River Laboratory. Humanized *Ugt1* (*hUGT1*)[30] mice were generated in our laboratory, in which mice carried the human *UGT1* transgene, which was expressed under a murine *Ugt1* null background. Global LXRα knockout ($Lxr\alpha^{-/-}$) mice[31] were originally developed by the David Mangelsdorf laboratory at the University of Texas Southwestern Medical Center, in which exons 3–6, containing the complete DNA-binding domain and majority of the ligand-binding domain, were replaced with a neomycin-resistance cassette. $Lxr\alpha^{-/-}$ mice were further crossbred into the *hUGT1* background for the generation of $Lxr\alpha^{-/-}/hUGT1$ ($Lxr\alpha^{-/-}/h$) mice. $Lxr\alpha^{-/-}/h$ mice of either sex were crossed with mice of the opposite sex carrying the heterozygous mutant allele ($Lxr\alpha^{+/-}/hUGT1$). $Atf4^{F/F}$ mice[32] were obtained from Christopher M. Adams at the University of Iowa, in which exons 2 and 3, the coding region of the mouse *Atf4* gene, was flanked with *LoxP* restriction sites. $Atf4^{F/F}$ mice were crossed with transgenic mice carrying Cre recombinase under control of the *Albumin* promoter (Strain 018961; Jackson Laboratory) to excise the floxed *Atf4* allele, and liver-specific ATF4-deficient mice ($Atf4^{\Delta Hep}$) were generated. $Atf4^{\Delta Hep}$ mice of either sex were crossed with $Atf4^{F/F}$ mice of the opposite sex. Both male and female pups 12–14 d of age with a BW of 4.0–8.0 g were included for all experiments, with siblings being preferred. Each treatment group consisted of at least three mice from at least two different litters. For *hUGT1* mice, a total of 163 mice were used: 11 for gut transit time measurement, 15 for immunochemical studies, 12 for time-dependent studies, 20 for dose-dependent studies, 24 for RNA-seq analysis, 28 for oleic acid (OA) and linoleic acid (LA) treatments, 12 for oral fat tolerance test (OFTT) studies, 16 for lipoprotein profile studies, and 25 for triple-dose treatment. In addition, 14 $Lxr\alpha^{+/-}/hUGT1$, 15 $Lxr\alpha^{-/-}/hUGT1$, 8 $Atf4^{F/F}$, 14 $Atf4^{\Delta Hep}$, and 8 WT C57BL/6J mice were used for the corresponding experiment. The exact number of replicates used for each outcome is specified in the corresponding figure legend. Mice were weaned at day 21.

All mouse strains were housed in a pathogen-free UCSD Animal Care Facility. All animal protocols were reviewed and approved by the UCSD Institutional Animal Care and Use Committee (IACUC). Mice in the present study had free access to autoclaved food and water *ad libitum*. The food was purchased from PicoLab (Rodent Diet 5053).

iAs and Treatments

Sodium arsenite (iAs; Sigma-Aldrich; Catalog no. S7400) was dissolved in drinking water at a concentration of 2 mg/mL and stored at 4°C. Each mouse received 5 μL/g BW of the prepared iAs solution by using a 22-gauge oral gavage needle (Fine Science Tools; Catalog no. 18061-22). For the single-dose treatment study, all mice mentioned above were treated by oral gavage with the vehicle (drinking water) or 10 mg/kg BW of iAs. For the dose-dependent study, mice were treated with iAs at doses of 1, 2, 5, and 10 mg/kg BW. Blood and tissue samples of the mice were collected 24 h postexposure. For the time-dependent study, neonatal *hUGT1* mice 14, 13, and 12 d of age were treated with 10 mg/kg BW of iAs, and samples were collected after 4, 24 and 48 h, respectively, so that mice at each time point were sacrificed at the same age of 14 d. For the triple-dose treatment study, 11-d-old *hUGT1* mice were orally treated with 10 mg/kg BW of iAs once per day, for 3 consecutive d. After 24 h following the last treatment, blood and liver tissue samples were obtained. For adult mouse studies, 8-wk-old male *hUGT1* mice were orally treated with either the vehicle or 10 mg/kg BW of iAs, and tissues were collected at 24 h after iAs treatment. For fatty acid (FA) treatment, 12-d-old *hUGT1* mice were gavaged with 10 g/kg BW of OA (Sigma-Aldrich; Catalog no. O1008) or 5 g/kg BW of LA (Sigma-Aldrich; Catalog no. L1376). Samples were collected 24 h later.

Blood Sample Collection

Mice were anesthetized by inhalation of isoflurane (Fluriso; VetOne; Catalog no. 502017). Blood samples were collected from the submandibular vein and centrifuged at $3,000 \times g$ for 3 min to obtain serum. The obtained serum samples were stored at −80°C until analysis.

Tissue Sample Collection for RNA, Protein, and Tissue Lysates

Liver tissues were dissected and washed with ice-cold phosphate-buffered saline (PBS; Gibco; Catalog no. 14190144). Small intestines were dissected, opened longitudinally, and washed with ice-cold PBS. After removing any excess PBS, the tissues were snap frozen in liquid nitrogen. The collected liver and small intestine tissues were pulverized in liquid nitrogen and stored at −80°C for further preparation of RNA, protein, and tissue lysates.

Tissue Sample Collection for Histology

Liver tissues were dissected and fixed in 10% phosphate-buffered formalin or embedded in Tissue-Tek optimum cutting temperature (O.C.T.) compound (Sakura; Catalog no. 4583) for frozen sectioning. Small intestines were dissected, washed with ice-cold PBS, and then prepared in a Swiss roll style for the same fixation process used for liver samples.

Enterocyte Isolation

The entire small intestine was dissected and cut longitudinally. After washing with PBS in 27 mM sodium citrate, the tissue was incubated in PBS with 2.5 mM ethylenediaminetetraacetic acid (EDTA; Bioworld; Catalog no. 40520000) at 4°C with shaking for 30 min. The tissue pieces were removed through filtration. The collected liquid was centrifuged at $1,000 \times g$ for 5 min to obtain the enterocytes. The cell pellets were resuspended in PBS buffer for sonication. After sonication, the resultant mixtures were centrifuged at $10,000 \times g$ for 10 min. The supernatants were collected and stored at −80°C for future studies.

Total Gut Transit Time Test

Neonatal mice were treated with vehicle or 10 mg/kg BW of iAs through oral gavage (Veh: $n = 5$, iAs: $n = 6$). After 24 h, the neonatal mice were separated from their dams. Each mouse was orally gavaged with 40 μL of carmine (0.3 mg in 0.5% methyl-cellulose; Sigma-Aldrich; Catalog no. C1022), and then the mice were placed in individual cages containing a white sheet of paper. The time taken for the first colored feces to be excreted was recorded.

OFTT

Neonatal 13-d-old mice were treated with the vehicle or 10 mg/kg BW of iAs via oral gavage. After 20 h, the treated mice were separated from their dams for a 5-h fast. Fasted mice were anesthetized using isoflurane inhalation and then injected with tyloxapol (Sigma-Aldrich; Catalog no. T0307) at 0.2 mg/g BW through a retro-orbital injection. Both vehicle and iAs-treated groups were further divided into two subgroups ($n = 3$). One subgroup was given water (50 μL per mouse) as a control group, whereas the other was given a single dose of corn oil (50 μL per mouse; Thermo Fisher Scientific; Catalog no. 405435000) via oral gavage. Blood samples were collected before and at 1, 2, and 3 h after water/corn oil treatment.

Serum Alanine Transaminase and Aspartate Aminotransferase Measurement

Preparation of serum was as described above. Alanine transaminase (ALT) and aspartate aminotransferase (AST) were measured using the ALT/GPT Reagent (Thermo Fisher Scientific; Catalog no. TR71121) and AST/GOT Reagent (Thermo Fisher Scientific; Catalog no. TR70121), following a colorimetric assay based on the manufacturer's instructions.

Lipid Measurement

Lipid in serum samples, enterocyte lysates, or liver tissue lysates were quantitated. Preparation of serum and enterocyte lysate was as described above. Liver tissue lysates were prepared by soni-cating ~ 100 mg of pulverized liver tissue in 100 μL of ice-cold PBS, followed by centrifugation at $10,000 \times g$ for 10 min. Lipids were measured by using a colorimetric assay based on the manufacturer's instructions, including the Triglyceride Colorimetric Assay Kit (Cayman Chemical; Catalog no. 10010303), the Free Fatty Acid Fluorometric Assay Kit (Cayman Chemical; Catalog no. 700310), and the Cholesterol Fluorometric Assay Kit (Cayman Chemical; Catalog no. 10007640). For serum samples, the results are described as amount per deciliter. For tissue lysates, results were normalized by protein concentration and are described as amount per gram of protein.

FPLC

Lipid profiling was carried out as previously described.[33] In brief, pooled serum samples from vehicle- and iAs-treated *hUGT1* mice were separated by gel-filtration FPLC through a GE Superose 6 10/30 GL column in 0.15 M sodium chloride containing 1 mM EDTA (Sigma-Aldrich) and 0.02% sodium azide (Sigma-Aldrich), pH 7.4. Fractions (0.5 mL) were collected at 0.5 mL/min. A total of 36 fractions were collected for each sample. Each fraction was used for measuring total cholesterol and triglyceride (TG) levels. For the western blot, 12 μL of each specified fraction was mixed with the lithium dodecyl sulfate (LDS) sample buffer and reducing agent (Thermo Fisher Scientific; Catalog no. J61942.AD) for denaturing gel electrophoresis.

RNA Preparation and Real-Time Quantitative Polymerase Chain Reaction

Approximately ~ 100 mg of pulverized liver or small intestine tissue powder was applied for total RNA isolation using 1 mL TRIzol reagent (Thermo Fisher Scientific; Catalog no. 15596026). The measurements of the amount and purity of the isolated RNA samples were performed on a NanoDrop Lite Spectrophotometer (Thermo Fisher Scientific). From 1 μg of total RNA, complementary DNA (cDNA) was generated using the iScript cDNA synthesis kit (Bio-Rad; Catalog no. 1708891), as outlined by the manufacturer. After synthesis of cDNA, 1 μL of the cDNA sample was used for polymerase chain reactions (PCRs) or real-time PCRs (RT-PCRs) conducted with Ssoadvanced Universal SYBR Green Supermix (Bio-Rad; Catalog no. 1725274), using a CFX96 Touch Real-Time PCR detection system (Bio-Rad; C1000 Touch Thermal Cycler; CFX96 Real-Time System) coupled with Bio-Rad CFX Manager 3.1 program. The cDNA template was analyzed in three steps following the PCR program: 1) denaturation at 95°C for 30 s; 2) 40 cycles of denaturation (at 95°C for 5 s) plus annealing/extension (at 60°C for 30 s) followed by plate read; and 3) melting curve analysis at 65–95°C (0.5°C increment, 5 s/step). The Ct values of the gene of interest were normalized to those of the mouse cyclophilin (*Cph*) gene. All primers used in this study were purchased from Integrated DNA Technologies, Inc., and are summarized in Table S1.

RNA-Seq Analysis Data Processing

Intestinal RNA was prepared from vehicle- and iAs-treated mice when they were 14-d old. RNA from three mice were pooled, and a total of four samples per group were used for RNA sequencing. The sequencing library was prepared using the Illumina Stranded mRNA Sample Prep Kit (Illumina; Catalog no. 20040534) with 1 μg of total RNA. Samples were sequenced with Paired End 100 base pair (PE100) sequencing on an Illumina NovaSeq6000 sequencer in the IGM Genomics Center at UCSD, with funding from a National Institutes of Health Shared Instrumentation Grant (SIG; #S10 OD026929). Base calling was performed using bcl2fastq (version 2.20; Illumina). STAR (version 2.7.9a) was used to align the RNA sequencing reads to the mouse genome (mm10) and to generate gene-level read counts from uniquely aligned reads. Differentially expressed genes were calculated with DESeq2 (version 1.34.0). The RNA-seq data generated in this study have been deposited in the Gene Expression Omnibus database: accession number GSE202602 (publicly available). Data generated with this study are available in the main text, as well as the figures and tables in the supplemental material.

Protein Preparation and Western Blot Analysis

Pulverized liver and small intestinal tissue samples (100 mg) were homogenized in 0.4 mL radioimmunoprecipitation assay buffer (RIPA) lysis buffer (EMD Millipore; Catalog no. 20-188) supplemented with a protease and phosphatase inhibitor cocktail (Thermo Fisher Scientific; Catalog nos. 87786 and 78420). The resultant mixture was centrifuged at $16,000 \times g$ for 20 min at 4°C and the supernatants were used for analysis. The protein concentrations were quantified using the Bradford protein assay (Bio-Rad; Catalog no. 5000006). Thirty micrograms of tissue-extracted protein was subject to electrophoresis in NuPAGE 4%–12% (or 3%–8%) BisTris-polyacrylamide gels (Thermo Fisher Scientific; Catalog no. NW04127BOX) and transferred to polyvinylidene fluoride (PVDF) membranes (EMD Millipore; Catalog no. IPVH00010). The membranes were blocked with 5% nonfat milk (Bio-Rad; Catalog no. 1706404) at room temperature for 1 h and incubated with primary antibodies at 4°C

overnight. All antibodies are listed in Table S2. The membranes were then washed and exposed to horseradish peroxidase–conjugated secondary antibodies (Cell Signaling Technology) for 1 h at room temperature. Protein was detected by the ECL Plus western Blotting Detection System (Bio-Rad; Catalog no.170-5061) and visualized using the Bio-Rad Chemidoc Touch Imaging System. We quantified the band densities, normalized them with glyceraldehyde 3-phosphate dehydrogenase (GAPDH), and demonstrated the results in fold change [mean $\pm$ standard error of the mean (SEM)].

Histology, Immunohistochemistry, and Oil Red O Staining

The mice were sacrificed, and the small intestine and liver tissues were fixed for subsequent paraffin embedding and sliced into 5-μm sections. A tissue histological examination was performed on the paraffin-embedded sections, which were stained with hematoxylin and eosin (H&E) and performed at the UCSD Cancer Center Histology Core. For Ki67 immunohistochemistry staining, paraffin-embedded sections of the small intestine were deparaffinized and treated with heat-mediated antigen retrieval using sodium citrate buffer (pH 6.0). After washing with PBS, the slides were incubated with 1% bovine serum albumin (Sigma-Aldrich; Catalog no. A7906) for 1 h at room temperature to block nonspecific binding. The slides were then incubated with anti-Ki67 antibody (Abcam; Catalog no. Ab-149; dilution factor, 1:100) overnight at 4°C. After washing, the slides were incubated for 1 h with Biotin Goat anti-Rabbit IgG Secondary Antibody (BD Pharmingen; Catalog no. 550338; dilution factor, 1:200). The intensity of indicated proteins was detected using the DAB Substrate Kit (Vector Laboratories Inc.; Catalog no. SK-4100).

For visualization of lipid droplets, intestinal and liver tissues were embedded in Tissue-Tek O.C.T. compound and placed immediately into a dry ice/iso-pentane slurry until it turned white. Cryo-sectioning was carried out at a thickness of 10 μm. Frozen slides were thawed at room temperature for several minutes and then fixed with 10% phosphate-buffered formalin. After washing, the slides were stained with freshly prepared Oil Red O working solution (0.3%; Sigma-Aldrich; Catalog no. O0625).

Photographs were examined using a 20×-Plan-Apochromat objective (numeric aperture, 0.8) on an upright Imager A2 microscope (Carl Zeiss Microscopy, LLC, White Plains, NY) with an Axiocam 506 color camera and ZEN2012 imaging software. More than six images at different areas were taken for each slide. For accurate enumeration, Ki67-positive (Ki67$^+$) cells were counted in at least 50 well-orientated villus-crypt units for each animal. Results were expressed as numbers of Ki67$^+$ cells per crypt. All cells were enumerated by at least two people who were not associated with this project, and data were collected in a double-blinded fashion.

Statistics

All statistics and graphs were generated using GraphPad Prism (version 9.3.1; GraphPad Software). For comparison between two groups, two-tailed unpaired Student's t-test or multiple unpaired t-tests analyses were performed. For multiple groups, one-way analysis of variance (ANOVA) with Tukey's multiple comparisons test was used to compare the mean of each column with the mean of every other column, whereas one-way ANOVA with Dunnett's multiple comparisons test was used to compare the mean of each group with the mean of the control group. A $p < 0.05$ was considered statistically significant, as indicated by asterisks in the figures ($^*p < 0.05$, $^{**}p < 0.01$, $^{***}p < 0.001$, $^{****}p < 0.0001$). All data are expressed as mean $\pm$ SEM.

Results

BW, Intestinal Weight, Gut Transit Time, and Intestinal Cell Proliferation in Neonatal Mice Exposed to a Single Dose of iAs at 10 mg/kg BW via Oral Gavage

Neonatal *hUGT1* mice were treated with either the vehicle or iAs at 10 mg/kg BW through oral gavage. Following 48 h of treatment, iAs-treated mice had $\sim 13.1\%$ ($p = 0.0182$) lower BW compared with vehicle-treated mice (Figure 1A). The small intestine was $\sim 9\%$ longer and 16% greater in weight in iAs-treated mice compared with vehicle-treated mice (Figure 1B–D). Twenty-four hours after iAs treatment, gut transit time was quantified by measuring the time interval taken for an oral dose of carmine red dye to appear in the stool. In iAs-treated mice, the gut transit time averaged 4.6 ± 0.6 h compared with 3.3 ± 0.3 h in vehicle-treated mice ($p = 0.0016$) (Figure 1E). Immunostaining of intestinal tissue with an antibody directed toward the antigen Ki-67, which is present in intestinal stem cells (ISCs) and transit amplifying cells, showed more Ki67$^+$ cells per crypt in iAs-treated mice (Figure 1F). Higher protein expression of the leucine-rich repeat-containing G protein-coupled receptor 5 (LGR5) protein, a selective marker of ISC,[34] and proliferating cell nuclear antigen (PCNA),[35] an indicator of accelerated cell cycle control at the G1/S transition phase, was also observed (Figure 1G; Figure S1). Sucrase isomaltase (SIS), a brush border glucosidase that is a marker for enterocyte maturation,[36] was induced at the transcriptional and protein levels (Figures 1G,H; Figure S1). In addition, gene expression of alkaline phosphatase 3 (*Akp3*), a duodenal-specific enterocyte maturation marker,[37] was also up-regulated (Figure 1H).

Lipids in the Small Intestine and Enterocytes in iAs-Treated Neonatal hUGT1 Mice, as Well as Intestinal Cell Proliferation following the Treatment of FA OA

After 24 h of iAs treatment, H&E staining of intestinal tissue demonstrated significant blebbing along the villi, particularly at the tip (Figure 2A). When the tissue sections were stained with Oil Red O, which detects neutral TGs and lipids, the blebbing structures illuminated bright red, indicating an accumulation of lipids on the apical surface of the small intestine after 24 h of iAs treatment (Figure 2B). When enterocyte lysates were prepared, a milky appearance was observed in samples from the iAs treatment (Figure 2C). Colorimetric analysis demonstrated a 5.6-fold higher concentration of TGs in iAs-treated animals compared with control mice ($p = 0.0001$) (Figure 2D), along with a 70% ($p = 0.0386$) more free FAs (FFAs) (Figure 2E). Intestinal cholesterol levels were similar between the two groups (Figure 2F). The expression of *Acly*, *Acaca*, *Fasn*, and *Scd1*, genes involved in *de novo* lipogenesis (DNL) was similar in the treated mice compared with the control group. At the same time, *Srebf1*, the key gene in controlling DNL, was expressed at a lower level at 4 and 24 h in iAs-treated mice compared with control mice (Figure S2A). These data led us to conclude that enterocyte lipid accumulation was driven by an increased accumulation of dietary fats from breast milk. We suspected that the active FAs in the accumulated lipids may promote intestinal growth, which in turn further enhances lipid absorption, forming a positive feedback loop driving the intestinal effects induced by iAs (Figure 2G). To examine this possibility, *hUGT1* neonatal mice were gavaged with OA (10 g/kg BW), an abundant monounsaturated FA (MUFA) in breastmilk.[38] Forty-eight hours post OA treatment, mice had significantly greater tissue weight than those treated with control ($p < 0.0001$) (Figure 2H), which correlated with the induction of intestinal epithelial cell (IEC) maturation markers SIS (*Sis*) and *Akp3*, along with the ISC marker LGR5 (Figure 2I–J; Figure S2B). Increased proliferation was further demonstrated by more Ki67$^+$
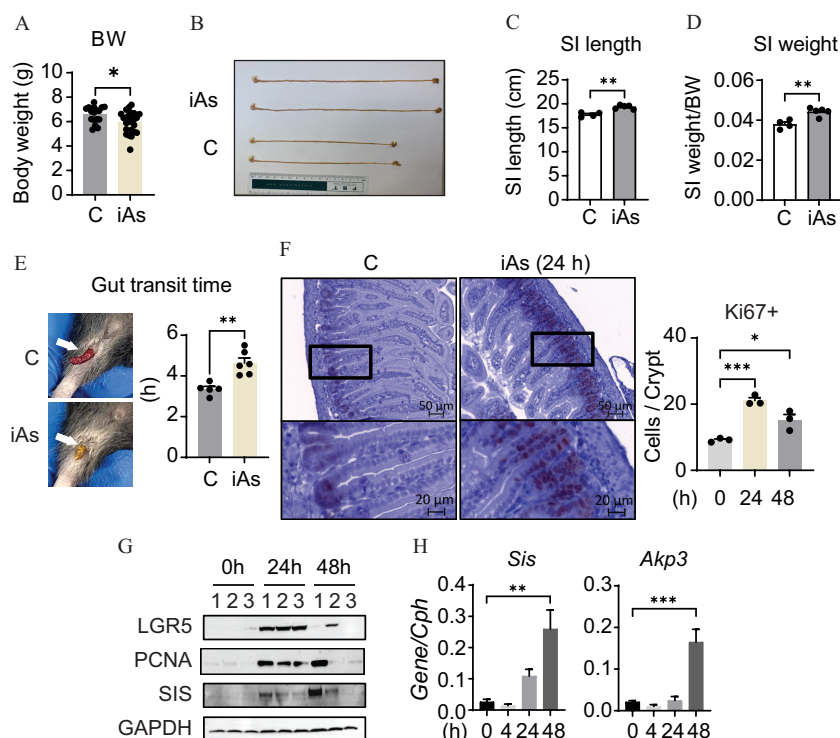
Figure 1. The morphological, cellular, and molecular changes of the small intestine in *hUGT1* neonatal mice after a single-dose iAs treatment at 10 mg/kg BW. Neonatal *hUGT1* mice (12–14 d old) were orally treated with control vehicle (C) or iAs (10 mg/kg BW) for various time points, and the mice were sacrificed at 14 d of age. (A) Mouse BW at 48 h after treatment ($n = 17$, 24, mean $\pm$ SEM, two-tailed Student's *t*-test). (B–D) Gross photo of small intestines at 48 h posttreatment, small intestine length and weight ($n = 4$, 5, mean $\pm$ SEM, two-tailed Student's *t*-test). (E) Gut transit time at 24 h after iAs treatment ($n = 5$, 6, mean $\pm$ SEM, two-tailed Student's *t*-test). (F) Immunostaining of Ki67. Ki67^{+} cells were enumerated and described as Ki67^{+} cells per crypt ($n = 3$, mean $\pm$ SEM, one-way ANOVA). Scale bars: 50 µm (upper) and 20 µm (lower). (G) Western blot analysis of intestinal LGR5, PCNA, and SIS at 24 and 48 h after iAs treatment. (H) RT-qPCR ($n = 3$, mean $\pm$ SEM). $^*p < 0.05$, $^{**}p < 0.01$, $^{***}p < 0.001$. Corresponding numeric data and individual *p*-values are listed in Excel Table S1. Note: Akp3, alkaline phosphatase 3; ANOVA, analysis of variance; BW, body weight; Cph, cyclophilin; GAPDH, glyceraldehyde 3-phosphate dehydrogenase; iAs, inorganic arsenic; Ki67^{+}, Ki67-positive; LGR5, leucine-rich repeat-containing G protein-coupled receptor 5; PCNA, proliferating cell nuclear antigen; RT-qPCR, real-time quantitative polymerase chain reaction; SEM, standard error of the mean; SI, small intestine; SIS, sucrase isomaltase.

cells per crypt (Figure 2K). Neonatal mice orally gavaged with LA, an essential polyunsaturated FA (PUFA) found in breast milk,[38] exhibited higher gene expression levels of *Sis* and *Akp3*, similar to the findings following OA treatment (Figure S2C).

RNA Sequencing Analysis of the Intestinal Tissue in Neonatal Mice Exposed to a Single Dose of iAs at 10 mg/kg BW via Oral Gavage

Intestinal RNA from control and iAs-treated *hUGT1* neonatal mice was subjected to whole-genome RNA sequencing (RNA-seq). With a threshold set at an absolute value of 1.5 and an adjusted *p*-value cutoff of 0.05, iAs treatment was associated with alterations in transcript abundance of 630 up-regulated and 611 down-regulated genes. Gene Ontology enrichment analysis showed that the five most up-regulated gene clusters in iAs-treated animals were glutathione metabolism, carboxylic acid metabolic processes, ribonucleoprotein complex biogenesis, cellular amide metabolic processes, and induction of mitotic anaphase (Figure 3A). On the other hand, the most down-regulated pathway involved the lysosome, the main intracellular digestive compartment for the degradation of macromolecules, including genes involved in formation of the lytic supranuclear vacuoles (*Slc46a3*, *Tmem9*, *Dab2*, *Mcoln3*, and *Glmp*), as well as genes related to the degradation of milk macromolecules within these vacuoles (*Hyal5*, several *Cts* genes, *Galns*, *Neu1*, *Lgmn*, *Lipa*, *Man2b2*) (Figure S3A).

A cluster of genes associated with lipid absorption was significantly down-regulated (Figure 3B), highlighted by those genes linked to chylomicron synthesis and cholesterol absorption.

Intestinal apolipoprotein B (*Apob*) gene expression was significantly down-regulated in iAs-treated animals. Other apolipoprotein genes typically associated with chylomicron assembly, including *Apoa1*, *Apoa4*, and *Apoc3*, were also down-regulated. The Niemann–Pick C1-like intracellular cholesterol transporter 1 (*Npc1l1*), a membrane protein that plays a critical role in the absorption of intestinal cholesterol,[39] was dramatically down-regulated (Figure 3B). Consistent with RNA-seq analysis, down-regulation of the *Npc1l1*, *Apob*, and *Apoa1* genes was also demonstrated by RT-qPCR in different segments of the small intestine (Figure 3C). For FA consumption, there were no significant differences observed in β-oxidation pathways (Figure S3B). However, expression of 3-hydroxy-3-methylglutaryl-CoA synthase 2 (*Hmgcs2*) gene, encoding the initial and rate-limiting enzyme for ketogenesis, was drastically lower in iAs-treated mice (Figure 3D). This finding was further confirmed at both the mRNA level and the protein level (Figures 3E–F, S3C). The intestinal *Hmgcs2* was abundantly expressed only in neonatal but not in adult mice (Figure S3D). Dose-dependent down-regulation of genes, including *Apob*, *Apoa1*, *Apoa4*, *Apoc3*, *Npc1l1*, and *Hmgcs2*, was also observed in mice treated with iAs ranging from 1 to 10 mg/kg BW (Figure S3E).

Lipids and Lipid Profiling in the Serum of iAs-Treated hUGT1 Neonatal Mice

Despite enterocyte lipid accumulation and impaired lipid absorption, when 13-d-old *hUGT1* mice were treated with iAs for 24 h followed by a 5-h fast, we observed an $\sim 180\%$ higher level of
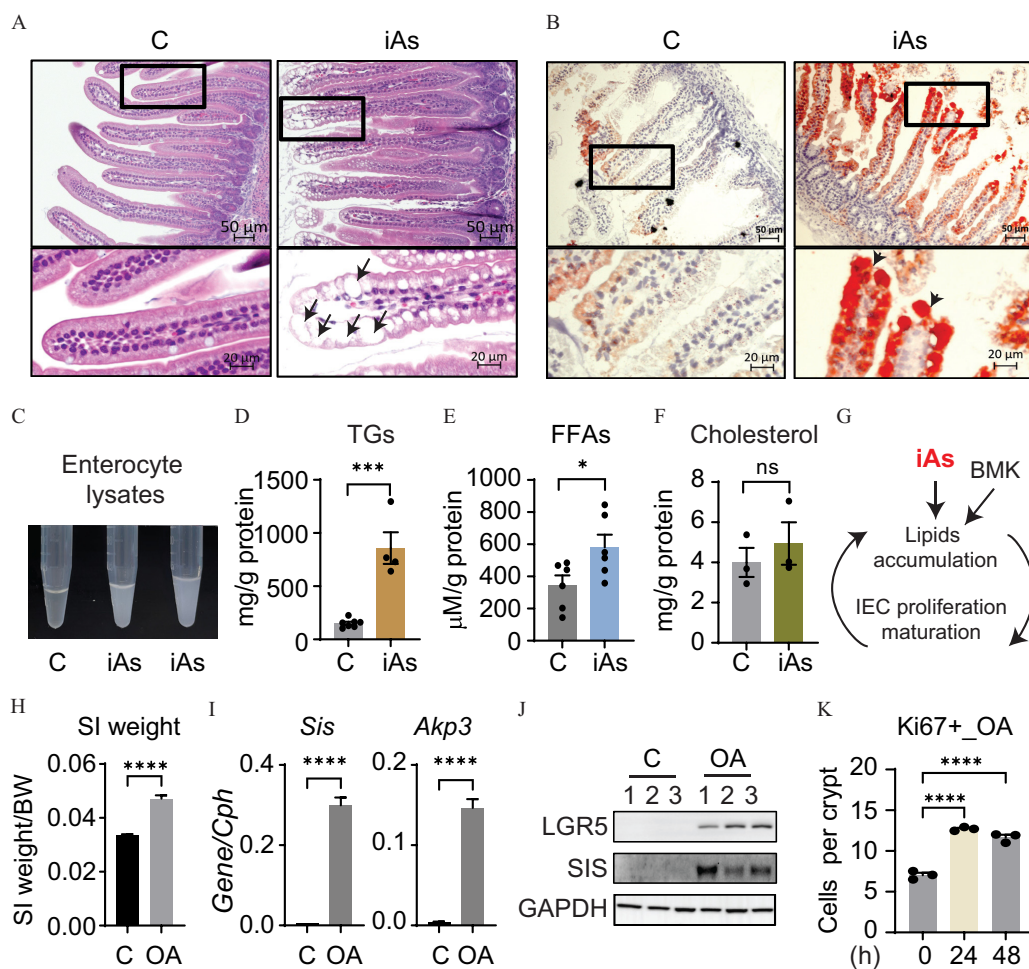
Figure 2. The lipid levels in enterocytes isolated from iAs-treated *hUGT1* neonatal mice, as well as the morphological, cellular, and molecular changes of *hUGT1* neonatal mice following treatment with OA. Neonatal *hUGT1* mice were orally treated with control vehicle (C) or iAs at 10 mg/kg BW. Small intestines were collected at 24 h and 48 h after treatment. Images were examined using a $20 \times$ Plan-Apochromat objective (numeric aperture, 0.8) on an upright Imager A2 microscope (Zeiss) with an Axiocam 506 color camera and ZEN2012 imaging software. Scale bars: 50 μm (upper) and 20 μm (lower). (A) Representative micrograph of H&E staining ($n = 3$). (B) Representative micrograph of Oil red O staining ($n = 3$). (C) Photos of aliquots of enterocyte lysates. (D–F) TGs ($n = 7$, 4, mean ± SEM, two-tailed Student's *t*-test), FFAs ($n = 6$, mean ± SEM, two-tailed Student's *t*-test), and cholesterol ($n = 3$, mean ± SEM) content in enterocytes. (G) Schematic description of the impact of iAs on lipids and IEC cell proliferation and maturation. (H–K) Neonatal *hUGT1* mice were orally treated with control vehicle (C) or OA at 10 g/kg BW. Small intestines were collected at 24 h and 48 h after treatment ($n = 8$, 5, mean ± SEM, two-tailed Student's *t*-test). (I) RT-qPCR at 48 h posttreatment, examining *Sis* and *Akp3* gene expression ($n = 8$, 5, mean ± SEM, two-tailed Student's *t*-test). (J) Western blot analysis of LGR5 and SIS. (K) Immunostaining of Ki67, Ki67$^+$ cells were enumerated and described as Ki67$^+$ cells per crypt ($n = 3$, mean ± SEM, one-way ANOVA). $^*p < 0.05$, $^{**}p < 0.01$, $^{***}p < 0.001$, $^{****}p < 0.0001$. Corresponding numeric data and individual *p*-values are listed in Excel Table S2. Note: Akp3, alkaline phosphatase 3; ANOVA, analysis of variance; BMK, breast milk; BW, body weight; Cph, cyclophilin; FFAs, free fatty acids; GAPDH, glyceraldehyde 3-phosphate dehydrogenase; H&E, hematoxylin and eosin; iAs, inorganic arsenic; IEC, intestinal epithelial cell; Ki67$^+$, Ki67-positive; LGR5, leucine-rich repeat-containing G protein-coupled receptor 5; OA, oleic acid; RT-qPCR, real-time quantitative polymerase chain reaction; SEM, standard error of the mean; SI, small intestine; SIS, sucrase isomaltase; TGs, triglycerides.

fasted serum TGs, along with an ∼70% higher level of serum FFAs (Figure 4A,B). Hypertriglyceridemia and higher serum FFAs were also observed at similar or greater levels after refeeding (Figure 4A,B). We then performed an OFTT, in which fasted mice were given corn oil via gavage along with retro-orbital injection of tyloxapol, which blocks lipoprotein lipase activity and TG clearance from the circulation.[40] A large increase in serum TGs at all time points were observed with a 3.9-fold higher value at 1 h post corn oil administration in iAs-treated mice, indicating a far greater secretion of TG-rich lipoprotein (TRL) (Figure 4C). In lipid profiling analysis by FPLC, the increase in fasting TG levels was reflected by a higher distribution to low-density lipoprotein (LDL)-sized remnant TRL particles (Figure 4D). In the fasted condition, the predominant lipoprotein was APOB100 in the TG-enriched fractions, which were higher in the iAs-exposed group (Figure 4D, fasting). Following refeeding, TGs shifted to the

very low-density lipoprotein (VLDL)/chylomicron remnant fraction (Figure 4D, TG-refed). Both APOB100 and APOB48 proteins were more highly expressed in the iAs-treated mice, with APOB100 being the dominant form (Figure 4D). In contrast to the higher level of TGs and FFAs, neonates with oral iAs exposure had significantly lower plasma cholesterol levels (Figure 4E), and the lower serum cholesterol level following a 2-h refeeding in the high-density lipoprotein (HDL) fraction is in accordance with the down-regulation of APOA1 (Figure 4F).

Lipid Levels in the Liver of *hUGT1* Neonatal Mice Treated with iAs

Liver tissues were collected 24 h after 13-d-old *hUGT1* mice were treated with iAs at 10 mg/kg BW via oral gavage. Liver TGs in iAs-treated mice were 40.4% greater than in vehicle-treated
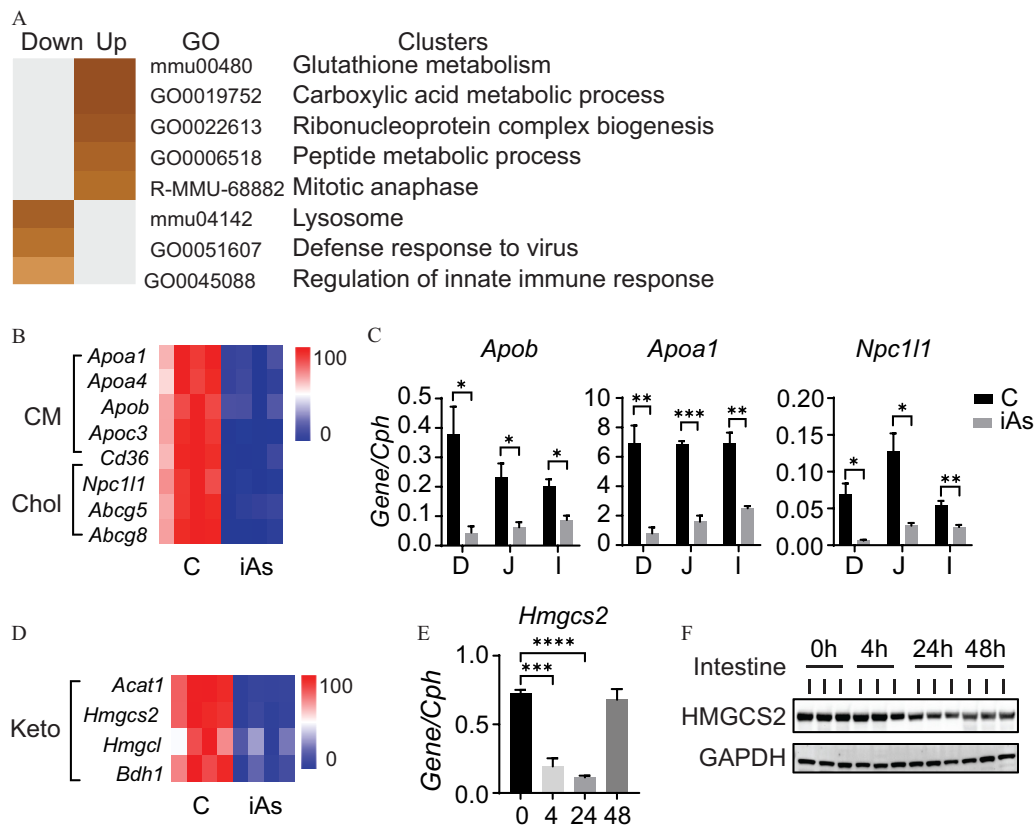
Figure 3. RNA sequencing and pathway analysis. Neonatal *hUGT1* mice 13 d of age were orally treated with control vehicle (C) or iAs at 10 mg/kg BW via oral gavage. Small intestines were collected 24 h after treatment. Total RNA samples from three mice were combined as one sample, with four samples from each group subjected for RNA-seq analysis. (A) Pathway analysis of control and iAs-treated mice. (B) Heat map comparing genes related to chylomicron synthesis and cholesterol absorption. (C) RT-qPCR of *Apob*, *Apoa1*, and *Npc1l1* gene expression from different sections of the small intestine, including duodenum (D), jejunum (J), and ileum (I) ($n = 3$, mean ± SEM, two-tailed Student's *t*-test). (D) Heat map comparing genes related to ketogenesis. (E) RT-qPCR of *Hmgcs2* gene expression over 48 h after treatment ($n = 3$, mean ± SEM, one-way ANOVA). (F) Western blot analysis of HMGCS2. $^{*}p < 0.05$, $^{**}p < 0.01$, $^{***}p < 0.001$, $^{****}p < 0.0001$. Corresponding numeric data and individual *p*-values are listed in Excel Table S3. Note: ANOVA, analysis of variance; Apoa1, apolipoprotein A1; Apob, apolipoprotein B; Chol, cholesterol; CM, chylomicrons; Cph, cyclophilin; D, duodenum; GAPDH, glyceraldehyde 3-phosphate dehydrogenase; GO, Gene Ontology; HMGCS2, 3-hydroxy-3-methylglutaryl-CoA synthase 2; I, ileum; iAs, inorganic arsenic; J, jejunum; Keto, ketogenesis; NPC1L1, NPC1 like intracellular cholesterol transporter 1; RNA-Seq, RNA sequencing; RT-qPCR, real-time quantitative polymerase chain reaction; SEM, standard error of the mean.

mice ($p = 0.0142$), with slightly more lipid droplets in Oil Red O staining (Figure 5A,B). Indications of hepatosteatosis were further evident when neonatal mice were treated with iAs for 3 consecutive d. Significant TG accumulation along with increased lipid droplet formation was observed in livers (Figure 5A,B), with a slightly higher ALT level after three doses, but AST showed no difference from control at either dose (Figure S4A). Animals exposed to acute iAs treatment did not exhibit significantly different mRNA levels of *Srebf1* or *Fasn* compared with control animals, suggesting that hepatic TG accumulation was not a result of DNL (Figure 5C; Figure S4B). However, stearoyl-CoA desaturase 1 (*Scd1*) and 2 (*Scd2*), enzymes that catalyze the conversion of saturated FAs to MUFAs were higher in iAs-treated mice (Figure 5C; Figure S4B), indicating increased exposure of saturated FAs to the liver.[41] Genes linked to FA uptake (*Fabp1* and *Cd36*), reesterification (*Dgat1/2* and *Mgat2*), or oxidation (*Cpt1a*, *Cyp4a10*, and *Cyp4a14*), showed no difference (Figure 5C; Figure S4C,D). Two genes associated with cholesterol synthesis were significantly up-regulated, *Srebf2* and the rate-limiting enzyme *Hmgcr* (Figure 5D). Cholesterol efflux transporters *Abcg5/8* in the liver were down-regulated, along with hepatic *Apoa1*, which could work in synergy with the down-regulation of intestinal *Apoa1* (Figure 5D). We noticed that hepatic *Apob* and *Apoa4* gene

expression, distinct from their down-regulated pattern observed in the small intestine (Figure 3B,C), showed no difference (*Apob*) or was significantly up-regulated (*Apoa4*) in the liver (Figure 5E). When we collected iAs-treated liver tissues for western blot analysis, a higher expression of APOB100 was observed in iAs-treated animals (Figure 5F; Figure S4E). Thus, different effects of iAs are expected due to the tissue-specific regulation of liver-derived APOB100 and intestinal-derived APOB48 (Figure 5G).

Lipid Accumulation in the Enterocyte and Enterocyte Maturation Were Examined in iAs-Treated *Lxrα⁻/⁻/hUGT1* Neonatal Mice

The liver X receptors (LXRs) are important regulators of intracellular cholesterol and lipid homeostasis.[31] RNA-seq data demonstrated that many of the LXR target genes, including *Srebf1*, *Abcg1*, *Abcg5*, *Abcg8*, and *Apoe*,[42] were significantly down-regulated in iAs-treated small intestinal tissue (Figure 6A), implying that iAs treatment was inhibiting LXR function. This observation led us to examine the impact of iAs on *Lxrα⁻/⁻* neonates. We have crossed *Lxrα⁻/⁻* mice into the *hUGT1* background and generated *Lxrα⁻/⁻/hUGT1* (*Lxrα⁻/⁻/h*) mice. The absence of LXRα expression was evident in both the liver and the small intestine in neonatal *Lxrα⁻/⁻/h* mice (Figure S5A). Control and *Lxrα⁻/⁻/h*
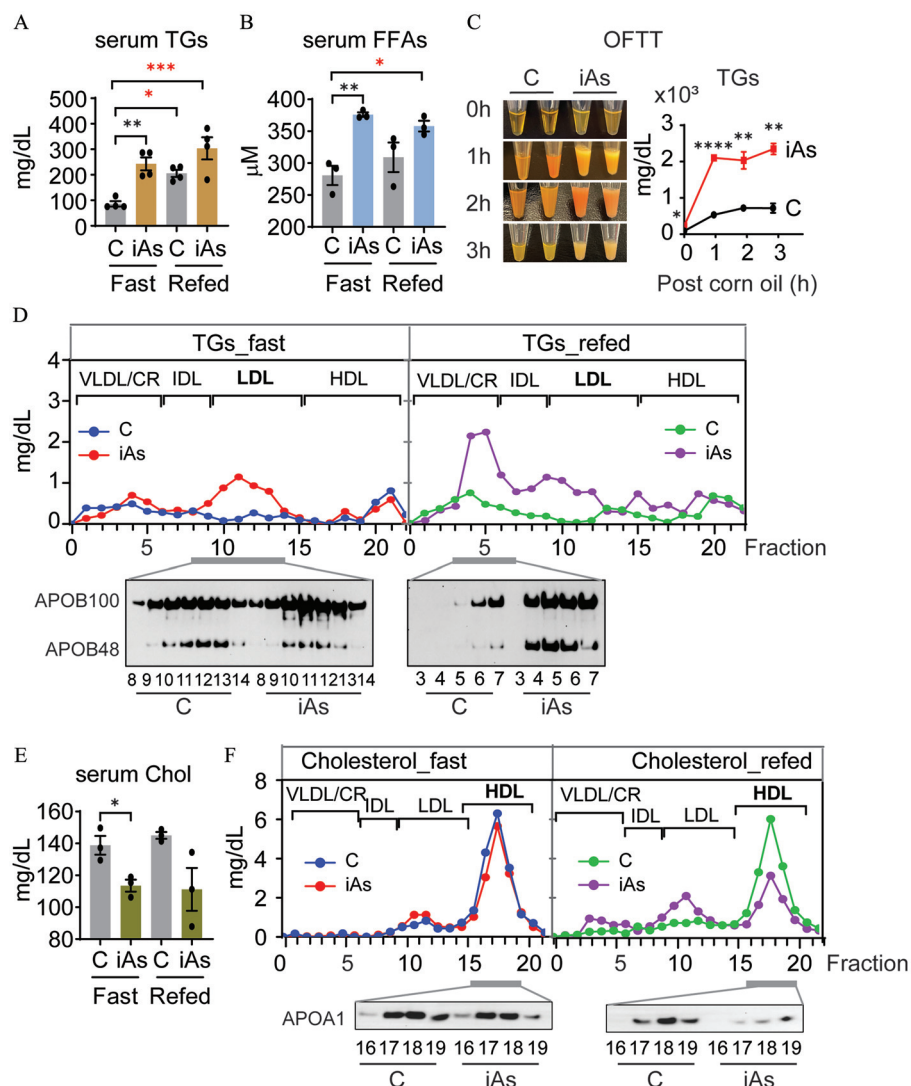
Figure 4. Serum lipid levels and lipoprotein profiles in iAs-treated *hUGT1* neonatal mice. Neonatal *hUGT1* mice at 13 d of age were orally treated with control vehicle (C) or iAs (10 mg/kg BW). After 24 h, mice were separated from the dams for a 5-h fast, and then refed for 2 h. (A,B) Fasted and refed serum TGs ($n = 4$, mean $\pm$ SEM, one-way ANOVA) and FFAs ($n = 3$, mean $\pm$ SEM, one-way ANOVA). (C) Neonatal mice were pretreated with control vehicle (C) or 10 mg/kg BW iAs for 20 h. After fasting for 5 h, mice received tyloxapol (0.2 mg/g given through retro-orbital injection) followed by oral gavage of corn oil (50 μL per mouse). Blood samples were collected at 1-, 2-, and 3-h posttreatment. Serum from two mice were pooled as one sample. Serum TG levels were measured ($n = 3$, mean $\pm$ SEM, multiple unpaired *t*-tests). (D) The lipoprotein profiles of serum from fasted and refed mice were pooled and analyzed using FPLC. The TGs in each fraction were measured. The elution positions of CR/VLDL, IDL, LDL, and HDL are indicated. The APOB100 and APOB48 protein levels in the selected fractions were measured by Western blot analysis. (E) Serum cholesterol levels from fasted and refed mice ($n = 3$, mean $\pm$ SEM, one-way ANOVA). (F) Cholesterol levels in each fraction were determined by FPLC. APOA1 protein levels in the selected fractions were measured by western blot analysis. $^{*}p < 0.05$, $^{**}p < 0.01$, $^{****}p < 0.0001$. Corresponding numeric data and individual *p*-values are listed in Excel Table S4. Note: ANOVA, analysis of variance; APOA, apolipoprotein A; APOB, apolipoprotein B; BW, body weight; Chol, cholesterol; CR, chylomicron remnant; FFAs, free fatty acids; FPLC, fast protein liquid chromatography; HDL, high-density lipoprotein; iAs, inorganic arsenic; IDL, intermediate-density lipoprotein; LDL, low-density lipoprotein; OFTT, oral fat tolerance test; TGs, triglycerides; VLDL, very low-density lipoprotein.

13-d-old neonates were treated with a single dose of iAs at 10 mg/kg BW via oral gavage. After 24 h, serum cholesterol levels were examined, and it was found that mice lacking LXRα exhibited similar levels of serum cholesterol when mice treated with iAs were compared to the mice treated with the vehicle (Figure 6B). Given that intestinal *Npc1l1* expression was similar in iAs-treated control and *Lxrα*$^{-/-}$/*h* mice (Figure 6C), this finding suggests that the LXRα deletion has no effect on cholesterol absorption in the intestine. However, a higher level of liver cholesterol was observed in iAs-treated *Lxrα*$^{-/-}$/*h* mice (Figure 6D). The liver is the principal site for converting cholesterol to bile acids for biliary excretion. The key protein in the control of cholesterol homeostasis is hepatic CYP7A1, a cholesterol 7α-hydroxylase

that catalyzes the rate-limiting step in converting cholesterol to bile acids. Western blot analysis confirmed that iAs-treated control mice exhibited slightly less CYP7A1 protein expression. However, iAs-treated *Lxrα*$^{-/-}$/*h* mice exhibited dramatically lower protein expression (Figure 6E; Figure S5B), thus counteracting the reduction in cholesterol absorption (Figure 6F). When we examined TG levels, there was super-induction of liver TGs in iAs-treated *Lxrα*$^{-/-}$/*h* mice compared with the control mice (Figure 6G). Concurrently, serum TGs were also hyperinduced in iAs-treated *Lxrα*$^{-/-}$/*h* mice (Figure 6H). Selective markers of intestinal maturation, such as the induction of *Sis* expression, and increased ISC marker LGR5, followed a similar super-induction profile (Figure 6I,J; Figure S5C).
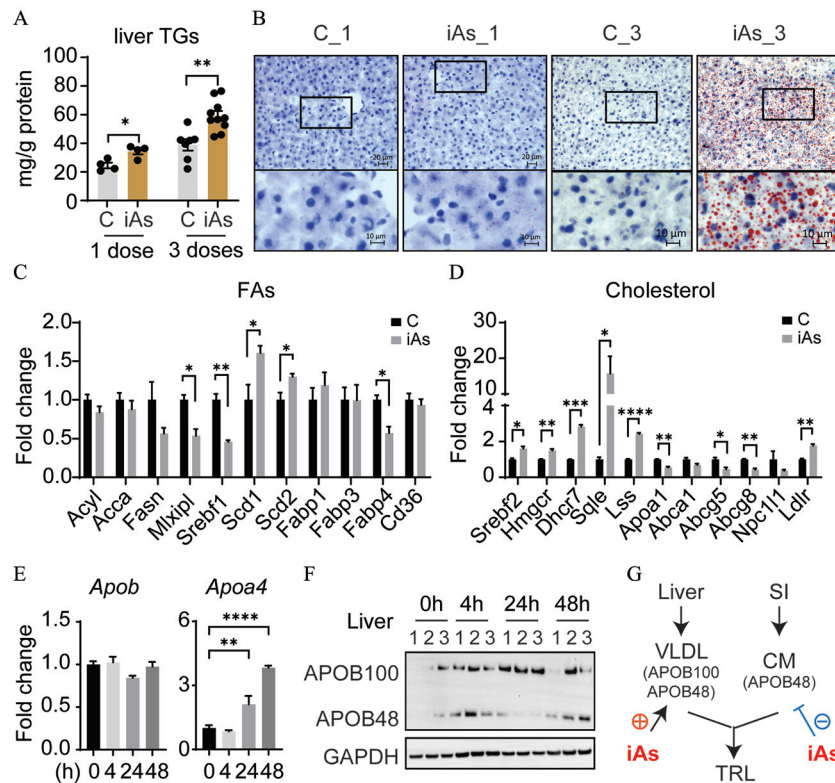
Figure 5. Liver lipid and hepatic *Apob* expression in iAs-treated *hUGT1* neonatal mice. (A,B) Single-dose treatment: Neonatal *hUGT1* mice 13 d of age were orally treated with a single dose of control vehicle (C) or iAs (10 mg/kg BW), and liver tissues were collected 24 h posttreatment. Three-dose treatment: Neonatal *hUGT1* mice 11 d of age were orally treated with control vehicle (C) or iAs at 10 mg/kg BW for 3 consecutive d. Twenty-four hours after the last treatment, liver samples were collected. (A) Liver TGs ($n = 4, 4, 7, 10$, mean ± SEM, two-tailed Student's *t*-test). (B) Oil Red O staining of liver samples. (C,D) Liver samples were collected after three doses of iAs treatment, RT-qPCR of genes related to FAs and cholesterol metabolism ($n = 3$, mean ± SEM, multiple unpaired *t*-tests). (E) RT-qPCR of *Apob* and *Apoa4* from mice with a single dose of iAs treatment ($n = 3$, mean ± SEM, one-way ANOVA). (F) Western blot analysis of APOB from liver samples. (G) Schematic description. $^*p < 0.05$, $^{**}p < 0.01$, $^{***}p < 0.001$, $^{****}p < 0.0001$. Corresponding numeric data and individual *p*-values are listed in Excel Table S5. Note: ANOVA, analysis of variance; Apoa, apolipoprotein A; Apob, apolipoprotein B, CM, chylomicron; FAs, fatty acids; GAPDH, glyceraldehyde 3-phosphate dehydrogenase; iAs, inorganic arsenic; RT-qPCR, real-time quantitative polymerase chain reaction; SEM, standard error of the mean; SI, small intestine; TGs, triglycerides; TRL, triglyceride-rich lipoprotein; VLDL, very low-density lipoprotein.

Endoplasmic Reticulum Stress, Lipids, and Enterocyte Maturation Examined in Neonatal Mice with or without Liver-Specific ATF4 Deletion

hUGT1 neonatal mice orally exposed to iAs for 24 h exhibited more protein kinase R (PKR)-like endoplasmic reticulum (ER) kinase (PERK) activation, as demonstrated by phosphorylation of the eukaryotic translation initiation factor 2 (eIF2α), and higher protein levels of activating transcription factor 4 (ATF4) (Figure 7A; Figure S6A). Following crossbreeding of floxed *Atf4* mice with Cre transgenic mice driven by the *Albumin* promoter (*Atf4^{ΔHep}* mice), ∼ 50% of ATF4 was deleted in the livers of neonates at 15 d of age (Figure S6B). *Atf4^{ΔHep}* mice treated with iAs exhibited lower gene expression of fibroblast growth factor 21 (*Fgf21*) and asparagine synthetase (*Asns*) compared with iAs-treated *Atf4^{F/F}* mice (Figure 7B). *Fgf21* and *Asns* are two genes known to be regulated by ATF4.[43,44] When compared with iAs-treated *Atf4^{F/F}* mice, iAs-treated *Atf4^{ΔHep}* mice showed no significant difference in liver or serum TG levels (Figure 7C,D). However, lower serum cholesterol levels following iAs treatment (compared with control) remained (Figure 7E). In contrast, the accumulation of TGs in enterocytes remained high in iAs-treated *Atf4^{ΔHep}* mice, along with greater expression of the maturation marker *Sis* expression and lower expression of intestinal *Apob* and *Apoa1* (Figure 7F,G).

The impact of iAs on lipid accumulation in the intestine, serum, and liver are pathological effects commonly observed in different murine models, including WT C57BL/6J mice. When WT C57BL/6J neonatal mice received either the vehicle or iAs at 10 mg/kg BW via oral gavage for 24 h, the iAs-treated mice showed higher levels of serum, enterocyte, and liver TGs, as well as lower serum cholesterol compared with the vehicle-treated control mice (Figure S7A,B). Furthermore, the iAs-treated mice demonstrated greater expression of the maturation marker *Sis* and lower expression of intestinal *Hmgcs2, Npc1l1, Apoa1, Apob* and *Apoc3* (Figure S7C), with similar *Apob* gene expression in the liver (Figure S7D), compared with untreated control mice.

Discussion

Our findings suggest that FFAs exhibited diverse and potent biological activities on IECs in a mouse model. To exaggerate the impact of FFAs on intestinal maturation, we treated neonatal mice with OA. The treatment reproduced the phenotypes observed after iAs exposure, including significantly greater intestinal growth, as well as greater IEC cell proliferation and enterocyte maturation. Given that OA is an abundant FA found in breast milk,[38] the authors hypothesize that OA exposure results in an accumulation of FFAs in enterocytes similar to what is observed following iAs treatment. We suggest that an overaccumulation of lipids in enterocytes drives cellular proliferation, intestinal growth, and IEC maturation. This was further supported using iAs-treated *Lxrα^{−/−}* mice, which exhibited greater lipid accumulation in concordance with
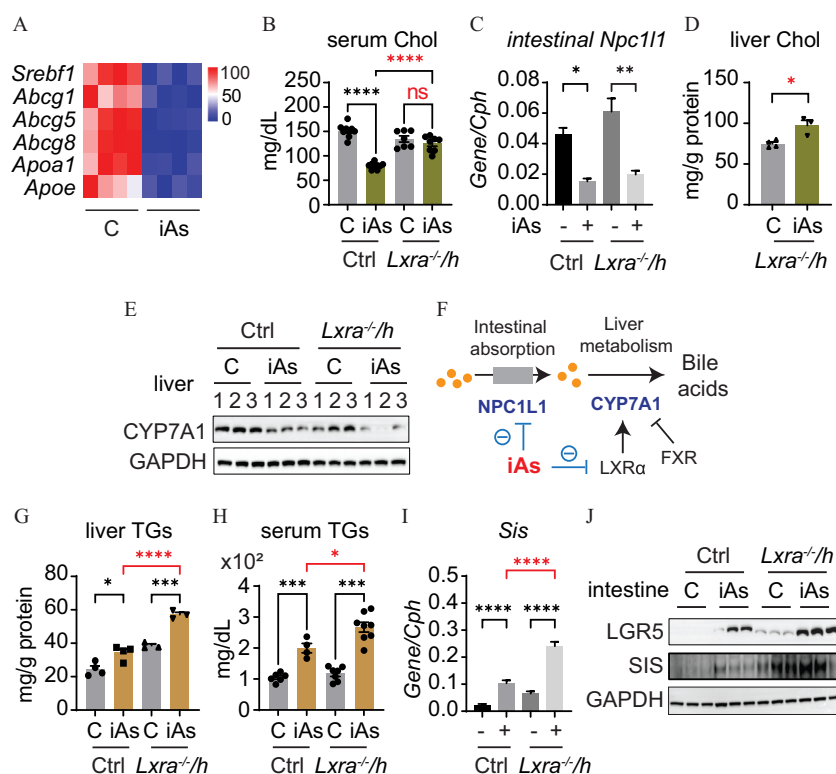
Figure 6. Lipid levels and intestinal growth in iAs-treated $Lxra^{-/-}$ neonatal mice. (A) Heat map comparing LXRα regulated genes from RNA-seq analysis. B–J Neonatal control ($Lxra^{+/-}/hUGT1$) and $Lxra^{-/-}/hUGT1$ ($Lxra^{-/-}/h$) mice were orally treated with control vehicle (C) or iAs at 10 mg/kg BW. After 24 h, the blood, small intestine, and liver samples were collected. (B) Serum cholesterol levels ($n = 7, 7, 7, 8$, mean ± SEM, one-way ANOVA). (C) RT-qPCR of $Npc1l1$ expression in intestinal tissue ($n = 3, 3, 4, 4$, mean ± SEM, one-way ANOVA). (D) Liver cholesterol levels ($n = 4, 3$, mean ± SEM, two-tailed Student's t-test) in $Lxra^{-/-}/h$ mice. (E) Western blot analysis of hepatic CYP7A1. (F) Schematic description. (G) Liver TG levels ($n = 4, 4, 3, 3$, mean ± SEM, one-way ANOVA). (H) Serum TG levels ($n = 6, 4, 7, 8$, mean ± SEM, one-way ANOVA). (I) RT-qPCR of the intestinal Sis gene ($n = 3$, mean ± SEM, one-way ANOVA). (J) Western blot analysis of intestinal LGR5 and SIS. $^*p < 0.05$, $^{**}p < 0.01$, $^{***}p < 0.001$, $^{****}p < 0.0001$. Corresponding numeric data and individual p-values are listed in Excel Table S6. Note: ANOVA, analysis of variance; Chol, cholesterol; Cntl, control; CYP7A1, a cholesterol 7α-hydroxylase; FXR, farnesoid X receptor; GAPDH, glyceraldehyde 3-phosphate dehydrogenase; iAs, inorganic arsenic; LGR5, leucine-rich repeat-containing G protein-coupled receptor 5; LXRα, liver X-receptor α; NPC1L1, Niemann–Pick C1-like intracellular cholesterol transporter 1; RNA-Seq, RNA sequencing; RT-qPCR, real-time quantitative polymerase chain reaction; SEM, standard error of the mean; SIS, sucrase isomaltase; TGs, triglycerides.

intensified IEC proliferation and maturation when compared with iAs-treated control mice. Recent findings that dietary fat is a factor in intestinal dysregulation support this conclusion,[45,46] wherein OA, FAs, or lipid mixtures augmented the numbers and function of Lgr5+ISCs in mice and *ex vivo* organoid cultures by activating peroxisome proliferator activated receptor delta (PPARδ) signaling.[45,46] It has yet to be explored whether PPARδ-dependent signaling serves any biological function in response to iAs exposure.

We observed that HMGCS2 protein expression was significantly lower in the small intestine following iAs exposure. HMGCS2 is the rate-limiting enzyme in ketogenesis, and its expression is confined within the liver and the intestinal tract.[47] Insufficient ketogenesis was shown to correlate with the degree of steatosis in patients with NAFLD.[48] We demonstrated that intestinal HMGCS2 was expressed abundantly only in neonates, but not in adult mice, confirming previous studies that had documented intestinal HMGCS2 was down-regulated after weaning.[49] This implies functional importance of intestinal HMGCS2 in the production of ketone bodies during the suckling period. Recent studies had found that ketogenesis plays a key role in protecting the energy-producing capacity of mitochondria in neonatal mice,[50] and mice lacking HMGCS2 developed a spontaneous FLD phenotype during postnatal development, which could be rescued via early weaning.[51] Further studies are required to support down-regulation of intestinal HMGCS2 as a pathological cause of iAs-induced NAFLD in early life.

In NAFLD, dyslipidemia is manifested as increased serum TG levels, increased numbers of small dense LDL particles, and decreased HDL-cholesterol levels, all of which are key risk factors for cardiovascular disease. In fact, cardiovascular disease is a leading cause of mortality in patients with NAFLD.[52] Our study demonstrated that mice treated with iAs exhibited postprandial hypertriglyceridemia, primarily from the overproduction of liver-derived VLDL. Notably, postprandial hypertriglyceridemia has been considered as one of the most important risk factors leading to atherosclerotic cardiovascular disease.[53] As the VLDL particles deliver TGs to the circulation, the hydrolysis of TGs is catalyzed by lipases in a process called lipolysis, resulting in the generation of intermediate-density lipoprotein (IDL) and then LDL particles.[53] Upon iAs treatment, TGs were enriched in LDL-sized TG-enriched particles, which can be used for producing small dense LDL-sized TRL remnants, featuring a decreased cholesterol-to-TG ratio with high atherogenicity.[54,55] In the postprandial state, TRLs consist of both intestinal-derived APOB48-containing chylomicrons and liver-derived APOB100-containing VLDL. APOB 48 is the major structural protein associated with chylomicron assembly. Chylomicrons are rapidly cleared from the circulation, but APOB48-containing VLDL accumulate and form a population of slowly cleared remnant particles.[56,57] It has been proposed that when chylomicron remnants are recycled into the liver, APOB48 may be reconstituted into VLDL and secreted from the liver as APOB48-VLDL.[58] However, in mice, this
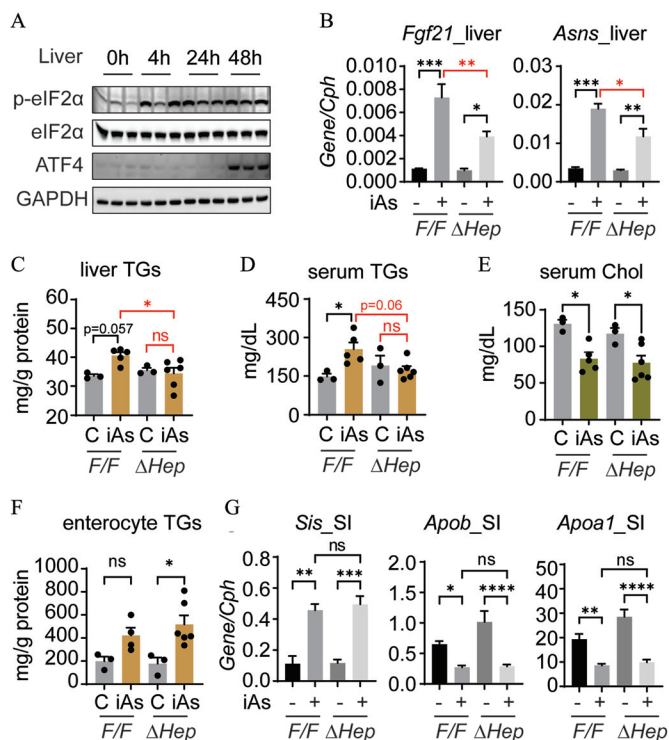
Figure 7. Liver ER stress in iAs-treated neonatal *hUGT1* mice; lipid levels, as well as *Fgf21*, *Asns*, *Sis*, *Apob*, and *Apoa1* gene expressions in iAs-treated *Atf4^ΔHep* mice. (A) Western blot analysis of liver samples collected from *hUGT1* neonatal mice following time-dependent iAs treatments. B–G 15-d-old *Atf4^F/F* and *Atf4^ΔHep* mice were orally treated with control vehicle (C) or iAs (10 mg/kg BW). After 24 h, blood, small intestine, and liver samples were collected ($n = 3, 5, 5, 3, 6$, one-way ANOVA). (B) RT-qPCR of ATF4 target genes, including *Fgf21* and *Asns* ($n = 3, 5, 5, 9$, mean ± SEM, one-way ANOVA). (C) Liver TG levels ($n = 3, 5, 3, 6$, mean ± SEM, one-way ANOVA). (D) serum TG levels ($n = 3, 5, 3, 6$, mean ± SEM, one-way ANOVA). (E) serum cholesterol levels ($n = 3, 5, 3, 6$, mean ± SEM, one-way ANOVA). (F) TG levels in enterocytes ($n = 3, 5, 3, 6$, mean ± SEM, one-way ANOVA). (G) RT-qPCR analysis of intestinal *Sis*, *Apob*, and *Apoa1* genes ($n = 3, 5, 5, 9$, mean ± SEM, one-way ANOVA). $^*p < 0.05$, $^{**}p < 0.01$, $^{***}p < 0.001$, $^{****}p < 0.0001$. Corresponding numeric data and individual *p*-values are listed in Excel Table S7. Note: ANOVA, analysis of variance; Apoa1, apolipoprotein A1; Apob, apolipoprotein B; Asns, asparagine synthetase; ATF4, activating transcription factor 4; Chol, cholesterol; Cph, cyclophilin; eIF2α, the eukaryotic translation initiation factor 2; ER, endoplasmic reticulum; *F/F*, *Atf4^F/F*; Fgf21, fibroblast growth factor 21; GAPDH, glyceraldehyde 3-phosphate dehydrogenase; ΔHep, *Atf4^ΔHep*; iAs, inorganic arsenic; RT-qPCR, real-time quantitative polymerase chain reaction; SEM, standard error of the mean; SI, small intestine; Sis, sucrase isomaltase; TGs, triglycerides.

concept becomes complicated because the liver can produce APOB48.[59] In addition to hypertriglyceridemia, the postprandial state induces multiple metabolic abnormalities, including hyperglycemia, oxidative stress, and increased levels of coagulation factors.[60] This could be further exaggerated in iAs exposure given that iAs itself generates reactive oxygen species (ROS) that lead to oxidative stress, as demonstrated by RNA-seq analysis studies showing induction of glutathione metabolism, a key indicator of ROS production. We have recently provided more direct evidence showing that iAs leads to the overexpression of NQO1, HMXO1, and GSTA1, the prototypical oxidative stress markers,[61] in both the liver and the intestine following iAs treatment in mice.[62] It has been previously reported that arsenic trioxide exposure led to the accumulation of cytotoxic levels of ceramide in acute promyelocytic leukemia and adult T-cell leukemia/lymphoma cells.[63] Bioactive ceramides have been shown to contribute to the development

of NALFD by increasing CD36-mediated lipid uptake and SREBP-mediated TG synthesis in mice.[64,65] In our study, under acute iAs exposure, both *Cd36* and *Srebpf1* were either not different or expressed at a lower level compared with vehicle-treated control mice, implying that ceramides are not likely to be the route accounting for iAs-induced NALFD.

Following exposure to iAs, RNA-seq analysis confirmed the down-regulation of *Apob* gene expression, which encodes APOB48 in the small intestine, a critical component of chylomicron assembly.[66] Human *APOB* gene mutations cause hypobetalipoproteinemia, a pathological condition that is diagnosed by the accumulation of fat in enterocytes.[67,68] The pathological similarity of iAs exposure blockage of murine *Apob* gene expression mimics what is seen in hypobetalipoproteinemia, blocking lipid transport out of the enterocytes, leading to the overaccumulation of dietary fats and lipids. We are not certain how iAs leads to enterocyte fat accumulation. One hypothesis is that the down-regulation of APOB48 hinders lipid lymphatic transport, allowing fat to accumulate in enterocytes, which then pushes FFAs through the portal vein to the liver, thus increasing hepatic TG synthesis and VLDL. Alternatively, iAs increases the fat supply to the intestines, resulting in a "traffic jam" given that chylomicron synthesis cannot meet the needs for transporting the accumulating fat from the intestines to the circulation. APOB100 is the structural protein involved in VLDL assembly. We demonstrated that oral iAs exposure had no effect on hepatic *Apob* transcription, but APOB100 protein expression was significantly higher compared with expression in control mice. Synthesis and secretion of APOB100 is largely controlled by protein degradation. APOB100 proteasomal degradation was initiated by p97, a cytosolic ATPase anchored to the ER membrane.[69] Recently, iAs was reported to compromise both p97 and proteasome functions.[70] Thus, iAs might increase APOB100 protein levels by slowing its degradation.

ER stress, which plays an important role in NAFLD, activates ATF4 through PERK.[71] ER stress and oxidative stress coexist in many pathologic states, with altered redox homeostasis induced by ROS sufficient to cause ER stress.[72] iAs is a potent ROS producer[73] and oxidative stress generator in the neonatal intestines, as demonstrated by RNA-seq data analysis. ER stress can lead to the activation of three effector pathways, including PERK, inositol-requiring enzyme 1 (IRE1), and ATF6. Recently, it was reported that iAs activated PERK-IRE1α-ATF6α signaling in iAs carcinogenesis.[74] In the rat hippocampus, iAs-induced learning and memory impairment through the activation of GRP78, CHOP, and the cleavage of caspase-12.[75] When neonates were challenged with oral iAs, western blot results showed that PERK became activated, as evidenced by phosphorylation of eIF2α and higher protein expression of ATF4. Employing *Atf4^ΔHep* mice, we found that elevated levels of liver and serum TGs, processes that can lead to NAFLD/TAFLD, were blocked. Recent studies have shown that whole-body *Atf4^−/−* mice exhibit increased FA oxidation and decreased FA synthesis.[76] It has also been demonstrated that CHOP binds directly to the C/EBP-binding regions in the promoters of target genes, repressing target gene expression, such as that initiated by PPARα.[77] Given that PPARα is the master regulator of FA oxidation,[78] it is possible that iAs exposure activates ER stress and compromises hepatic lipid expenditure through eIF2α-ATF4-directed inhibition of PPARα, leading to TG accumulation and NAFLD/TAFLD. We demonstrated that *Lxrα^−/−* mice were more sensitive to iAs-induced hypertriglyceridemia, with higher TGs and FFA levels in both serum and liver samples. LXRα played an important role in mice in protecting the liver from saturated FA-induced ER stress.[79] Thus, the absence of LXRα may exacerbate TG accumulation by exaggerating liver ER stress. LXRα is a cellular oxysterol sensor that stimulates CYP7A1

transcription,[31] the rate-limiting step of the classic pathway of bile acid synthesis. In addition, CYP7A1 is also negatively regulated by the bile acid sensor farnesoid X receptor (FXR).[80] When LXRα is deleted, repressive regulation by FXR could dominate, resulting in diminished expression of CYP7A1, which would lead to reduced conversion of cholesterol to bile acids. This may counteract the reduction in cholesterol absorption following iAs treatment, resulting in a reduced decrease of the cholesterol level in mice lacking *Lxrα*.

iAs exposure has been demonstrated to be lifelong, starting *in utero*.[10,11] More recently, *in utero* and "whole life" exposure models have been used to examine NAFLD. Using *in utero* exposure only, offspring of dams with iAs exposure at 100 ppb (from gestation day 6 to term) have been shown to develop NAFLD in 36 wk.[81] The offspring exhibited increased blood sugar levels and elevated LDL and total cholesterol levels. Atherosclerosis-prone *Apoe*$^{-/-}$ mice that were exposed to 49 ppm iAs *in utero* showed no macroscopic histological changes in liver after 10 wk, although both ALT and AST levels were increased, indicating liver damage.[82] Ditzel reported[83,84] that when mice were maintained on a high-fat diet and co-treated with iAs, mice with *in utero* and continuous early life exposure to iAs developed more severe NAFLD pathology compared with those with *in utero* iAs exposure only, implying the importance of postnatal exposure of iAs in the development of NAFLD. This has been supported by our findings that acute iAs exposure via oral administration to neonatal mice induced hepatosteatosis, the early stages of NAFLD. In addition, iAs exposure during the lactational stage induced the rapid accumulation of dietary fat in enterocytes, a unique phenotypical change that in turn accelerated intestinal growth and enterocyte maturation. These new studies have associated enterocyte lipid accumulation with iAs-induced hepatosteatosis and serum lipoprotein abnormalities, highlighting the importance of the intestinal tract and the gut–liver axis in mediating iAs-NAFLD.

In this study, iAs was administered orally via gavage to neonatal mice during the suckling period, mimicking what occurs to human infants who are primarily exposed to iAs through contaminated drinking water, formula, and other infant foods. iAs exposure levels vary greatly for humans depending on their diet and living conditions. The European Food Safety Authority (EFSA) estimated that dietary exposure to iAs in children <3 years of age was 0.50–2.66 μg/kg BW per day,[14] but in heavily polluted areas, such as southwestern Taiwan, the Niigata Prefecture in Japan, and Northern Chile,[85] along with Guizhou in China[86] and Bangladesh,[87] the iAs levels in food can reach up to 4 mg/kg BW and to >100 ppb in the drinking water. If 7.5-kg infants consume daily 35 g of solid baby food and 1 L of iAs-contaminated groundwater, the approximate total exposure level in these areas could easily reach up to 20 μg/kg BW per day. In addition, mice are known to have a significantly higher tolerance for detoxifying iAs than humans owing to the high activity of arsenite methyltransferase (AS3MT), which catalyzes arsenic methylation.[88,89] Therefore, the use of doses up to 100 ppm for long-term iAs treatments have been reported in experimental mouse studies.[90–93] Taking all of the above factors into consideration, together with a correction factor (K_M) of 12.3 based on body surface area,[94] a single dose of 1–10 mg/kg BW iAs via oral gavage was applied in this study.

Mice with a C57BL/6J background were used in this study. It is important to note that most of the data obtained using *hUGT1* mice are associated with the *hUGT1* background (*Lxrα*$^{-/-}$/*hUGT1*), with the exception of *Atf4*$^{F/F}$ and *Atf4*$^{\Delta Hep}$ mice. *hUGT1* mice were developed in our laboratory as a murine model mimicking the clinical observations of neonatal hyperbilirubinemia.[30] However, the impact of iAs on the development of hyperlipidemia is independent of neonatal hyperbilirubinemia or the genetic background associated with *hUGT1* mice. This is supported by data observed in

Atf4$^{F/F}$ and *Atf4*$^{\Delta Hep}$ mice, strains with no *hUGT1* background, in which all of the key markers, including lipid accumulation in enterocytes, accelerated enterocyte maturation, hypertriglyceridemia, as well as hepatosteatosis, were observed. Furthermore, using WT C57BL/6J mice, we also reproduced many of the key experiments associated with lipid disruption using WT C57BL/6J neonatal mice.

In conclusion, iAs exposure during the suckling period led to enterocyte fat accumulation, serum lipoprotein abnormalities, and atherogenic dyslipidemia, which included hypertriglyceridemia, decreased HDL-C, and the early stages of NAFLD. These pathophysiological alterations illustrated the importance of the gut–liver axis and a potential linkage toward the regulation of ER stress. With iAs exposure occurring *in utero* and often continuing through adulthood, constant iAs exposure in combination with a high caloric diet that includes excessive fats and sugar, may promote precocious development of FLD in adolescents. Greater clarity is also emerging implicating prenatal iAs exposure with the onset of chronic adult diseases.[95]

References

1. Ravenscroft P, Brammer H, Richards K. 2009. *Arsenic Pollution: A Global Synthesis*. Chichester, UK: Wiley-Blackwell.
2. Rahman MM, Sengupta MK, Ahamed S, Lodh D, Das B, Hossain MA, et al. 2005. Murshidabad—one of the nine groundwater arsenic-affected districts of West Bengal, India. Part I: magnitude of contamination and population at risk. Clin Toxicol (Phila) 43(7):823–834, PMID: 16440510, https://doi.org/10.1080/15563650500357461.
3. U.S. EPA (U.S. Environmental Protection Agency). 2000. *Arsenic Occurrence in Public Drinking Water Supplies*. EPA-815-R-00-23. Washington, DC: U.S. EPA.
4. Huq SMI, Joardar JC, Parvin S, Correll R, Naidu R. 2006. Arsenic contamination in food-chain: transfer of arsenic into food materials through groundwater irrigation. J Health Popul Nutr 24(3):305–316, PMID: 17366772.
5. Wilson D. 2015. Arsenic consumption in the United States. J Environ Health 78(3):8–14, PMID: 26591332.
6. Sun GX, Williams PN, Zhu YG, Deacon C, Carey AM, Raab A, et al. 2009. Survey of arsenic and its speciation in rice products such as breakfast cereals, rice crackers and Japanese rice condiments. Environ Int 35(3):473–475, PMID: 18775567, https://doi.org/10.1016/j.envint.2008.07.020.
7. Jackson BP, Taylor VF, Karagas MR, Punshon T, Cottingham KL. 2012. Arsenic, organic foods, and brown rice syrup. Environ Health Perspect 120(5):623–626, PMID: 22336149, https://doi.org/10.1289/ehp.1104619.
8. Gilbert-Diamond D, Cottingham KL, Gruber JF, Punshon T, Sayarath V, Gandolfi AJ, et al. 2011. Rice consumption contributes to arsenic exposure in US women. Proc Natl Acad Sci USA 108(51):20656–20660, PMID: 22143778, https://doi.org/10.1073/pnas.1109722108.
9. Williams PN, Villada A, Deacon C, Raab A, Figuerola J, Green AJ, et al. 2007. Greatly enhanced arsenic shoot assimilation in rice leads to elevated grain levels compared with wheat and barley. Environ Sci Technol 41(19):6854–6859, PMID: 17969706, https://doi.org/10.1021/es070627i.
10. Punshon T, Davis MA, Marsit CJ, Theiler SK, Baker ER, Jackson BP, et al. 2015. Placental arsenic concentrations in relation to both maternal and infant biomarkers of exposure in a US cohort. J Expo Sci Environ Epidemiol 25(6):599–603, PMID: 25805251, https://doi.org/10.1038/jes.2015.16.

11. Guan H, Piao F, Zhang X, Li X, Li Q, Xu L, et al. 2012. Prenatal exposure to arsenic and its effects on fetal development in the general population of Dalian. Biol Trace Elem Res 149(1):10–15, PMID: 22451376, https://doi.org/10.1007/s12011-012-9396-7.

12. Ershow AB, Cantor KP. 1989. *Total Water and Tapwater Intake in the United States: Population-Based Estimates of Quantities and Sources*. Bethesda, MD: Life Sciences Research Office, Federation of American Societies for Experimental Biology.

13. Landrigan PJ, Suk WA, Amler RW. 1999. Chemical wastes, children's health, and the Superfund Basic Research Program. Environ Health Perspect 107(6):423–427, PMID: 10339440, https://doi.org/10.1289/ehp.99107423.

14. EFSA Panel on Contaminants in the Food Chain. 2009. Scientific opinion on arsenic in food. EFSA J 7(10):1351, https://doi.org/10.2903/j.efsa.2009.1351.

15. Del Rio M, Alvarez J, Mayorga T, Dominguez S, Sobin C. 2017. A comparison of arsenic exposure in young children and home water arsenic in two rural West Texas communities. BMC Public Health 17(1):850, PMID: 29078766, https://doi.org/10.1186/s12889-017-4808-4.

16. Rehm J, Samokhvalov AV, Shield KD. 2013. Global burden of alcoholic liver diseases. J Hepatol 59(1):160–168, PMID: 23511777, https://doi.org/10.1016/j.jhep.2013.03.007.

17. Zhang X, Ji X, Wang Q, Li JZ. 2018. New insight into inter-organ crosstalk contributing to the pathogenesis of non-alcoholic fatty liver disease (NAFLD). Protein Cell 9(2):164–177, PMID: 28643267, https://doi.org/10.1007/s13238-017-0436-0.

18. Schwingel PA, Cotrim HP, Salles BR, Almeida CE, dos Santos CR Jr, Nachef B, et al. 2011. Anabolic-androgenic steroids: a possible new risk factor of toxicant-associated fatty liver disease. Liver Int 31(3):348–353, PMID: 21040407, https://doi.org/10.1111/j.1478-3231.2010.02346.x.

19. Tuomisto S, Huhtala H, Martiskainen M, Goebeler S, Lehtimäki T, Karhunen PJ, et al. 2019. Age-dependent association of gut bacteria with coronary atherosclerosis: tampere sudden death study. PLoS One 14(8):e0221345, PMID: 31437200, https://doi.org/10.1371/journal.pone.0221345.

20. Loomba R, Friedman SL, Shulman GI. 2021. Mechanisms and disease consequences of nonalcoholic fatty liver disease. Cell 184(10):2537–2564, PMID: 33989548, https://doi.org/10.1016/j.cell.2021.04.015.

21. Sweeny KF, Lee CK. 2021. Nonalcoholic fatty liver disease in children. Gastroenterol Hepatol (NY) 17(12):579–587, PMID: 35465068.

22. Tamaki N, Ajmera V, Loomba R. 2022. Non-invasive methods for imaging hepatic steatosis and their clinical importance in NAFLD. Nat Rev Endocrinol 18(1):55–66, PMID: 34815553, https://doi.org/10.1038/s41574-021-00584-0.

23. Kabarra K, Golabi P, Younossi ZM. 2021. Nonalcoholic steatohepatitis: global impact and clinical consequences. Endocr Connect 10(10):R240–R247, PMID: 34486981, https://doi.org/10.1530/EC-21-0048.

24. Wahlang B, Beier JI, Clair HB, Bellis-Jones HJ, Falkner KC, McClain CJ, et al. 2013. Toxicant-associated steatohepatitis. Toxicol Pathol 41(2):343–360, PMID: 23262638, https://doi.org/10.1177/0192623312468517.

25. Rajak S, Raza S, Tewari A, Sinha RA. 2022. Environmental toxicants and NAFLD: a neglected yet significant relationship. Dig Dis Sci 67(8):3497–3507, PMID: 34383198, https://doi.org/10.1007/s10620-021-07203-y.

26. Frediani JK, Naioti EA, Vos MB, Figueroa J, Marsit CJ, Welsh JA, et al. 2018. Arsenic exposure and risk of nonalcoholic fatty liver disease (NAFLD) among U.S. adolescents and adults: an association modified by race/ethnicity, NHANES 2005–2014. Environ Health 17(1):6, PMID: 29334960, https://doi.org/10.1186/s12940-017-0350-1.

27. Nobili V, Alisi A, Newton KP, Schwimmer JB. 2016. Comparison of the phenotype and approach to pediatric vs adult patients with nonalcoholic fatty liver disease. Gastroenterology 150(8):1798–1810, PMID: 27003600, https://doi.org/10.1053/j.gastro.2016.03.009.

28. Schwimmer JB, Behling C, Newbury R, Deutsch R, Nievergelt C, Schork NJ, et al. 2005. Histopathology of pediatric nonalcoholic fatty liver disease. Hepatology 42(3):641–649, PMID: 16116629, https://doi.org/10.1002/hep.20842.

29. Africa JA, Behling CA, Brunt EM, Zhang N, Luo Y, Wells A, et al. 2018. In children with nonalcoholic fatty liver disease, zone 1 steatosis is associated with advanced fibrosis. Clin Gastroenterol Hepatol 16(3):438–446.e1, PMID: 28286193, https://doi.org/10.1016/j.cgh.2017.02.030.

30. Fujiwara R, Nguyen N, Chen S, Tukey RH. 2010. Developmental hyperbilirubinemia and CNS toxicity in mice humanized with the *UDP glucuronosyltransferase 1* (*UGT1*) locus. Proc Natl Acad Sci USA 107(11):5024–5029, PMID: 20194756, https://doi.org/10.1073/pnas.0913290107.

31. Peet DJ, Turley SD, Ma W, Janowski BA, Lobaccaro JM, Hammer RE, et al. 1998. Cholesterol and bile acid metabolism are impaired in mice lacking the nuclear oxysterol receptor LXR alpha. Cell 93(5):693–704, PMID: 9630215, https://doi.org/10.1016/s0092-8674(00)81432-4.

32. Ebert SM, Dyle MC, Kunkel SD, Bullard SA, Bongers KS, Fox DK, et al. 2012. Stress-induced skeletal muscle Gadd45a expression reprograms myonuclei and causes muscle atrophy. J Biol Chem 287(33):27290–27301, PMID: 22692209, https://doi.org/10.1074/jbc.M112.374777.

33. Gordts PLSM, Nock R, Son NH, Ramms B, Lew I, Gonzales JC, et al. 2016. ApoC-III inhibits clearance of triglyceride-rich lipoproteins through LDL family receptors. J Clin Invest 126(8):2855–2866, PMID: 27400128, https://doi.org/10.1172/JCI86610.

34. Barker N, van Es JH, Kuipers J, Kujala P, van den Born M, Cozijnsen M, et al. 2007. Identification of stem cells in small intestine and colon by marker gene *Lgr5*. Nature 449(7165):1003–1007, PMID: 17934449, https://doi.org/10.1038/nature06196.

35. Kelman Z. 1997. PCNA: structure, functions and interactions. Oncogene 14(6):629–640, PMID: 9038370, https://doi.org/10.1038/sj.onc.1200886.

36. Triadou N, Zweibaum A. 1985. Maturation of sucrase-isomaltase complex in human fetal small and large intestine during gestation. Pediatr Res 19(1):136–138, PMID: 3969306, https://doi.org/10.1203/00006450-198501000-00035.

37. Narisawa S, Hoylaerts MF, Doctor KS, Fukuda MN, Alpers DH, Millán JL, et al. 2007. A novel phosphatase upregulated in *Akp3* knockout mice. Am J Physiol Gastrointest Liver Physiol 293(5):G1068–G1077, PMID: 17901166, https://doi.org/10.1152/ajpgi.00073.2007.

38. Koletzko B. 2016. Human milk lipids. Ann Nutr Metab 69(suppl 2):28–40, PMID: 28103608, https://doi.org/10.1159/000452819.

39. Altmann SW, Davis HR Jr, Zhu LJ, Yao X, Hoos LM, Tetzloff G, et al. 2004. Niemann-Pick C1 like 1 protein is critical for intestinal cholesterol absorption. Science 303(5661):1201–1204, PMID: 14976318, https://doi.org/10.1126/science.1093131.

40. Rasouli M, Tahmouri H, Mosavi-Mehr M. 2016. The long term kinetic of plasma lipids and lipoproteins in tyloxapol injected rats. J Clin Diagn Res 10(6):BF01–BF05, PMID: 27504278, https://doi.org/10.7860/JCDR/2016/18890.7993.

41. Matsui H, Yokoyama T, Sekiguchi K, Iijima D, Sunaga H, Maniwa M, et al. 2012. Stearoyl-CoA desaturase-1 (SCD1) augments saturated fatty acid-induced lipid accumulation and inhibits apoptosis in cardiac myocytes. PLoS One 7(3):e33283, PMID: 22413010, https://doi.org/10.1371/journal.pone.0033283.

42. Repa JJ, Mangelsdorf DJ. 2002. The liver X receptor gene team: potential new players in atherosclerosis. Nat Med 8(11):1243–1248, PMID: 12411951, https://doi.org/10.1038/nm1102-1243.

43. Maruyama R, Shimizu M, Li J, Inoue J, Sato R. 2016. *Fibroblast growth factor 21* induction by activating transcription factor 4 is regulated through three amino acid response elements in its promoter region. Biosci Biotechnol Biochem 80(5):929–934, PMID: 27010621, https://doi.org/10.1080/09168451.2015.1135045.

44. Balasubramanian MN, Butterworth EA, Kilberg MS. 2013. Asparagine synthetase: regulation by cell stress and involvement in tumor biology. Am J Physiol Endocrinol Metab 304(8):E789–E799, PMID: 23403946, https://doi.org/10.1152/ajpendo.00015.2013.

45. Beyaz S, Mana MD, Roper J, Kedrin D, Saadatpour A, Hong SJ, et al. 2016. High-fat diet enhances stemness and tumorigenicity of intestinal progenitors. Nature 531(7592):53–58, PMID: 26935695, https://doi.org/10.1038/nature17173.

46. Luo C, Puigserver P. 2016. Stem cells: dietary fat promotes intestinal dysregulation. Nature 531(7592):42–43, PMID: 26935693, https://doi.org/10.1038/531042a.

47. Puchalska P, Crawford PA. 2017. Multi-dimensional roles of ketone bodies in fuel metabolism, signaling, and therapeutics. Cell Metab 25(2):262–284, PMID: 28178565, https://doi.org/10.1016/j.cmet.2016.12.022.

48. Mooli RGR, Ramakrishnan SK. 2022. Emerging role of hepatic ketogenesis in fatty liver disease. Front Physiol 13:946474, PMID: 35860662, https://doi.org/10.3389/fphys.2022.946474.

49. Williamson DH, Thornton PS. 2004. Chapter 43 - Ketone body production and metabolism in the fetus and neonate. In: *Fetal and Neonatal Physiology*, 3rd ed. Polin RA, Fox WW, Abman SH, eds. Philadelphia, PA: W.B. Saunders, 419–428.

50. Arima Y, Nakagawa Y, Takeo T, Ishida T, Yamada T, Hino S, et al. 2021. Murine neonatal ketogenesis preserves mitochondrial energetics by preventing protein hyperacetylation. Nat Metab 3(2):196–210, PMID: 33619377, https://doi.org/10.1038/s42255-021-00342-6.

51. Asif S, Kim RY, Fatica T, Sim J, Zhao X, Oh Y, et al. 2022. Hmgcs2-mediated ketogenesis modulates high-fat diet-induced hepatosteatosis. Mol Metab 61:101494, PMID: 35421611, https://doi.org/10.1016/j.molmet.2022.101494.

52. Zhang QQ, Lu LG. 2015. Nonalcoholic fatty liver disease: dyslipidemia, risk for cardiovascular complications, and treatment strategy. J Clin Transl Hepatol 3(1):78–84, PMID: 26357637, https://doi.org/10.14218/JCTH.2014.00037.

53. Ginsberg HN, Packard CJ, Chapman MJ, Borén J, Aguilar-Salinas CA, Averna M, et al. 2021. Triglyceride-rich lipoproteins and their remnants: metabolic insights, role in atherosclerotic cardiovascular disease, and emerging therapeutic strategies-a consensus statement from the European Atherosclerosis Society. Eur Heart J 42(47):4791–4806, PMID: 34472586, https://doi.org/10.1093/eurheartj/ehab551.

54. Boren J, Lee I, Zhu W, Arnold K, Taylor S, Innerarity TL, et al. 1998. Identification of the low density lipoprotein receptor-binding site in apolipoprotein B100 and the modulation of its binding activity by the carboxyl terminus in familial defective apo-B100. J Clin Invest 101(5):1084–1093, PMID: 9486979, https://doi.org/10.1172/JCI1847.

55. Hurt-Camejo E, Camejo G, Sartipy P. 2000. Phospholipase A2 and small, dense low-density lipoprotein. Curr Opin Lipidol 11(5):465–471, PMID: 11048889, https://doi.org/10.1097/00041433-200010000-00004.

56. Björnson E, Packard CJ, Adiels M, Andersson L, Matikainen N, Söderlund S, et al. 2019. Investigation of human apoB48 metabolism using a new, integrated non-steady-state model of apoB48 and apoB100 kinetics. J Intern Med 285(5):562–577, PMID: 30779243, https://doi.org/10.1111/joim.12877.

57. Björnson E, Packard CJ, Adiels M, Andersson L, Matikainen N, Söderlund S, et al. 2020. Apolipoprotein B48 metabolism in chylomicrons and very low-density lipoproteins and its role in triglyceride transport in normo- and hypertri-glyceridemic human subjects. J Intern Med 288(4):422–438, PMID: 31846520, https://doi.org/10.1111/joim.13017.

58. Nakajima K, Tokita Y, Tanaka A. 2019. Hypothesis II: the majority of VLDL-apoB48 remnants in postprandial plasma are derived from the liver, not from the intestine. Clin Chim Acta 490:12–16, PMID: 30553860, https://doi.org/10.1016/j.cca.2018.12.010.

59. Greeve J, Altkemper I, Dieterich JH, Greten H, Windler E. 1993. Apolipoprotein B mRNA editing in 12 different mammalian species: hepatic expression is reflected in low concentrations of apoB-containing plasma lipoproteins. J Lipid Res 34(8):1367–1383, PMID: 8409768, https://doi.org/10.1016/S0022-2275(20)36966-2.

60. Borén J, Taskinen MR, Björnson E, Packard CJ. 2022. Metabolism of triglyceride-rich lipoproteins in health and dyslipidaemia. Nat Rev Cardiol 19(9):577–592, PMID: 35318466, https://doi.org/10.1038/s41569-022-00676-y.

61. Ma Q. 2013. Role of nrf2 in oxidative stress and toxicity. Annu Rev Pharmacol Toxicol 53:401–426, PMID: 23294312, https://doi.org/10.1146/annurev-pharmtox-011112-140320.

62. Yang X, Weber AA, Mennillo E, Paszek M, Wong S, Le S, et al. 2023. Oral arsenic administration to *humanized UDP-glucuronosyltransferase* 1 neonatal mice induces UGT1A1 through a dependence on Nrf2 and PXR. J Biol Chem 299(3):102955, PMID: 36720308, https://doi.org/10.1016/j.jbc.2023.102955.

63. Dbaibo GS, Kfoury Y, Darwiche N, Panjarian S, Kozhaya L, Nasr R, et al. 2007. Arsenic trioxide induces accumulation of cytotoxic levels of ceramide in acute promyelocytic leukemia and adult T-cell leukemia/lymphoma cells through de novo ceramide synthesis and inhibition of glucosylceramide synthase activity. Haematologica 92(6):753–762, PMID: 17550847, https://doi.org/10.3324/haematol.10968.

64. Chaurasia B, Tippetts TS, Mayoral Monibas R, Liu J, Li Y, Wang L, et al. 2019. Targeting a ceramide double bond improves insulin resistance and hepatic steatosis. Science 365(6451):386–392, PMID: 31273070, https://doi.org/10.1126/science.aav3722.

65. Jiang C, Xie C, Li F, Zhang L, Nichols RG, Krausz KW, et al. 2015. Intestinal farnesoid X receptor signaling promotes nonalcoholic fatty liver disease. J Clin Invest 125(1):386–402, PMID: 25500885, https://doi.org/10.1172/JCI76738.

66. Lo CC, Coschigano KT. 2020. ApoB48 as an efficient regulator of intestinal lipid transport. Front Physiol 11:796, PMID: 32733283, https://doi.org/10.3389/fphys.2020.00796.

67. Cefalù AB, Pirruccello JP, Noto D, Gabriel S, Valenti V, Gupta N, et al. 2013. A novel APOB mutation identified by exome sequencing cosegregates with steatosis, liver cancer, and hypocholesterolemia. Arterioscler Thromb Vasc Biol 33(8):2021–2025, PMID: 23723369, https://doi.org/10.1161/ATVBAHA.112.301101.

68. Desomer L, De Vos M, De Looze D. 2015. Fat accumulation in enterocytes: a key to the diagnosis of abetalipoproteinemia or homozygous hypobetalipoproteinemia. Endoscopy 47(suppl 1 UCTN):E223–E224, PMID: 26062159, https://doi.org/10.1055/s-0034-1391832.

69. Rutledge AC, Qiu W, Zhang R, Kohen-Avramoglu R, Nemat-Gorgani N, Adeli K, et al. 2009. Mechanisms targeting apolipoprotein B100 to proteasomal degradation: evidence that degradation is initiated by BiP binding at the N terminus and the formation of a p97 complex at the C terminus. Arterioscler Thromb Vasc Biol 29(4):579–585, PMID: 19164805, https://doi.org/10.1161/ATVBAHA.108.181859.

70. Tillotson J, Zerio CJ, Harder B, Ambrose AJ, Jung KS, Kang M, et al. 2017. Arsenic compromises both p97 and proteasome functions. Chem Res Toxicol 30(7):1508–1514, PMID: 28636814, https://doi.org/10.1021/acs.chemrestox.7b00158.

71. Pakos-Zebrucka K, Koryga I, Mnich K, Ljujic M, Samali A, Gorman AM, et al. 2016. The integrated stress response. EMBO Rep 17(10):1374–1395, PMID: 27629041, https://doi.org/10.15252/embr.201642195.

72. Cao SS, Kaufman RJ. 2014. Endoplasmic reticulum stress and oxidative stress in cell fate decision and human disease. Antioxid Redox Signal 21(3):396–413, PMID: 24702237, https://doi.org/10.1089/ars.2014.5851.

73. Jomova K, Jenisova Z, Feszterova M, Baros S, Liska J, Hudecova D, et al. 2011. Arsenic: toxicity, oxidative stress and human disease. J Appl Toxicol 31(2):95–107, PMID: 21321970, https://doi.org/10.1002/jat.1649.

74. Wadgaonkar P, Chen F. 2021. Connections between endoplasmic reticulum stress-associated unfolded protein response, mitochondria, and autophagy in arsenic-induced carcinogenesis. Semin Cancer Biol 76:258–266, PMID: 33836253, https://doi.org/10.1016/j.semcancer.2021.04.004.

75. Sun H, Yang Y, Shao H, Sun W, Gu M, Wang H, et al. 2017. Sodium arsenite-induced learning and memory impairment is associated with endoplasmic reticulum stress-mediated apoptosis in rat hippocampus. Front Mol Neurosci 10:286, PMID: 28936164, https://doi.org/10.3389/fnmol.2017.00286.

76. Wang C, Huang Z, Du Y, Cheng Y, Chen S, Guo F, et al. 2010. ATF4 regulates lipid metabolism and thermogenesis. Cell Res 20(2):174–184, PMID: 20066008, https://doi.org/10.1038/cr.2010.4.

77. Chikka MR, McCabe DD, Tyra HM, Rutkowski DT. 2013. C/EBP homologous protein (CHOP) contributes to suppression of metabolic genes during endoplasmic reticulum stress in the liver. J Biol Chem 288(6):4405–4415, PMID: 23281479, https://doi.org/10.1074/jbc.M112.432344.

78. Kersten S. 2014. Integrated physiology and systems biology of PPARα. Mol Metab 3(4):354–371, PMID: 24944896, https://doi.org/10.1016/j.molmet.2014.02.002.

79. Rong X, Albert CJ, Hong C, Duerr MA, Chamberlain BT, Tarling EJ, et al. 2013. LXRs regulate ER stress and inflammation through dynamic modulation of membrane phospholipid composition. Cell Metab 18(5):685–697, PMID: 24206663, https://doi.org/10.1016/j.cmet.2013.10.002.

80. Wang J, Einarsson C, Murphy C, Parini P, Björkhem I, Gåfvels M, et al. 2006. Studies on LXR- and FXR-mediated effects on cholesterol homeostasis in normal and cholic acid-depleted mice. J Lipid Res 47(2):421–430, PMID: 16264196, https://doi.org/10.1194/jlr.M500441-JLR200.

81. Sanchez-Soria P, Broka D, Quach S, Hardwick RN, Cherrington NJ, Camenisch TD, et al. 2014. Fetal exposure to arsenic results in hyperglycemia, hypercholesterolemia, and nonalcoholic fatty liver disease in adult mice. J Toxicol Health 1(1):1, https://doi.org/10.7243/2056-3779-1-1.

82. States JC, Singh AV, Knudsen TB, Rouchka EC, Ngalame NO, Arteel GE, et al. 2012. Prenatal arsenic exposure alters gene expression in the adult liver to a proinflammatory state contributing to accelerated atherosclerosis. PLoS One 7(6):e38713, PMID: 22719926, https://doi.org/10.1371/journal.pone.0038713.

83. Ditzel EJ, Nguyen T, Parker P, Camenisch TD. 2016. Effects of arsenite exposure during fetal development on energy metabolism and susceptibility to diet-induced fatty liver disease in male mice. Environ Health Perspect 124(2):201–209, PMID: 26151952, https://doi.org/10.1289/ehp.1409501.

84. Ditzel EJ, Li H, Foy CE, Perrera AB, Parker P, Renquist BJ, et al. 2016. Altered hepatic transport by fetal arsenite exposure in diet-induced fatty liver disease. J Biochem Mol Toxicol 30(7):321–330, PMID: 26890134, https://doi.org/10.1002/jbt.21796.

85. Celik I, Gallicchio L, Boyd K, Lam TK, Matanoski G, Tao X, et al. 2008. Arsenic in drinking water and lung cancer: a systematic review. Environ Res 108(1):48–55, PMID: 18511031, https://doi.org/10.1016/j.envres.2008.04.001.

86. Liu J, Zheng B, Aposhian HV, Zhou Y, Chen ML, Zhang A, et al. 2002. Chronic arsenic poisoning from burning high-arsenic-containing coal in Guizhou, China. Environ Health Perspect 110(2):119–122, PMID: 11836136, https://doi.org/10.1289/ehp.02110119.

87. Das HK, Mitra AK, Sengupta PK, Hossain A, Islam F, Rabbani GH, et al. 2004. Arsenic concentrations in rice, vegetables, and fish in Bangladesh: a preliminary study. Environ Int 30(3):383–387, PMID: 14987870, https://doi.org/10.1016/j.envint.2003.09.005.

88. Koller BH, Snouwaert JN, Douillet C, Jania LA, El-Masri H, Thomas DJ, et al. 2020. Arsenic metabolism in mice carrying a *BORCS7/AS3MT* locus humanized by syntenic replacement. Environ Health Perspect 128(8):87003, PMID: 32779937, https://doi.org/10.1289/EHP6943.

89. Douillet C, Miller M, Cable PH, Shi Q, El-Masri H, Matoušek T, et al. 2023. Fate of arsenicals in mice carrying the human *AS3MT* gene exposed to environmentally relevant levels of arsenite in drinking water. Sci Rep 13(1):3660, PMID: 36871058, https://doi.org/10.1038/s41598-023-30723-8.

90. Tokar EJ, Diwan BA, Ward JM, Delker DA, Waalkes MP. 2011. Carcinogenic effects of "whole-life" exposure to inorganic arsenic in CD1 mice. Toxicol Sci 119(1):73–83, PMID: 20937726, https://doi.org/10.1093/toxsci/kfq315.

91. Waalkes MP, Ward JM, Liu J, Diwan BA. 2003. Transplacental carcinogenicity of inorganic arsenic in the drinking water: induction of hepatic, ovarian, pulmonary, and adrenal tumors in mice. Toxicol Appl Pharmacol 186(1):7–17, PMID: 12583988, https://doi.org/10.1016/s0041-008x(02)00022-4.

92. Waalkes MP, Ward JM, Diwan BA. 2004. Induction of tumors of the liver, lung, ovary and adrenal in adult mice after brief maternal gestational exposure to inorganic arsenic: promotional effects of postnatal phorbol ester exposure on hepatic and pulmonary, but not dermal cancers. Carcinogenesis 25(1):133–141, PMID: 14514661, https://doi.org/10.1093/carcin/bgg181.

93. Tokar EJ, Diwan BA, Waalkes MP. 2010. Arsenic exposure in utero and nonepidermal proliferative response in adulthood in Tg.AC mice. Int J Toxicol 29(3):291–296, PMID: 20448261, https://doi.org/10.1177/1091581810362804.

94. Nair AB, Jacob S. 2016. A simple practice guide for dose conversion between animals and human. J Basic Clin Pharm 7(2):27–31, PMID: 27057123, https://doi.org/10.4103/0976-0105.177703.

95. Young JL, Cai L, States JC. 2018. Impact of prenatal arsenic exposure on chronic adult diseases. Syst Biol Reprod Med 64(6):469–483, PMID: 29873257, https://doi.org/10.1080/19396368.2018.1480076.